

# Two temperature accretion around rotating black holes: Description of general advective flow paradigm in presence of various cooling processes to explain low to high luminous sources

S. R. Rajesh\*, Banibrata Mukhopadhyay†

*Astronomy and Astrophysics Program, Department of Physics, Indian Institute of Science, Bangalore 560012, India*

3 September 2018

## ABSTRACT

We investigate the viscous two temperature accretion disc flows around rotating black holes. We describe the global solution of accretion flows with a sub-Keplerian angular momentum profile, by solving the underlying conservation equations including explicit cooling processes selfconsistently. Bremsstrahlung, synchrotron and inverse Comptonization of soft photons are considered as possible cooling mechanisms. We focus on the set of solutions for sub-Eddington, Eddington and super-Eddington mass accretion rates around Schwarzschild and Kerr black holes with a Kerr parameter 0.998. It is found that the flow, during its infall from the Keplerian to sub-Keplerian transition region to the black hole event horizon, passes through various phases of advection – general advective paradigm to radiatively inefficient phase and vice versa. Hence the flow governs much lower electron temperature  $\sim 10^8 - 10^{9.5}$ K, in the range of accretion rate in Eddington units  $0.01 \lesssim \dot{M} \lesssim 100$ , compared to the hot protons of temperature  $\sim 10^{10.2} - 10^{11.8}$ K. Therefore, the solution may potentially explain the hard X-rays and  $\gamma$ -rays emitted from AGNs and X-ray binaries. We then compare the solutions for two different regimes of viscosity and conclude that a weakly viscous flow is expected to be cooling dominated, particularly at the inner region of the disc, compared to its highly viscous counter part which is radiatively inefficient. With all the solutions in hand, we finally reproduce the observed luminosities of the under-fed AGNs and quasars (e.g. Sgr A\*) to ultra-luminous X-ray sources (e.g. SS433), at different combinations of input parameters such as mass accretion rate, ratio of specific heats. The set of solutions also predicts appropriately the luminosity observed in the highly luminous AGNs and ultra-luminous quasars (e.g. PKS 0743-67).

**Key words:** accretion, accretion disc — black hole physics — hydrodynamics — radiative transfer

## 1 INTRODUCTION

The cool Keplerian accretion disc (Pringle & Rees 1972; Shakura & Sunyaev 1973; Novikov & Thorne 1973) was found to be inappropriate to explain observed hard X-rays, e.g. from Cyg X-1 (Lightman & Shapiro 1975). It was argued that secular instability of the cool disc swells the optically thick, radiation dominated region to a hot, optically thin, gas dominated region resulting in hard component of spectrum  $\sim 100$ KeV (Thorne & Price 1975; Shapiro, Lightman & Eardley 1976). This region is strictly of two temperatures with electron and ion temperatures respectively  $\sim 10^9$ K and  $\sim 5 \times 10^{11}$ K which confirms that cool, one temperature, pure Keplerian accretion solution is not unique. Indeed Eardley & Lightman (1975) found that a Keplerian disc is unstable due to thermal and viscous effects when viscosity parameter  $\alpha$  (Shakura & Sunyaev 1973) is constant. Later Eggum et al. (1985) showed by numerical simulations that the Keplerian disc with a constant  $\alpha$  collapses.

Around eighties, therefore, the idea of two component accretion disc started floating around. For example, Paczyński & Wiita (1980) described a geometrically thick regime of the accretion disc in the optically thick limit, while Rees et al. (1982) introduced accretion torus in

\* rajesh@physics.iisc.ernet.in

† bm@physics.iisc.ernet.in

the optically thin limit. Moreover the idea of sub-Keplerian, transonic accretion was introduced by Muchotrzeb & Paczyński (1982), which was later improved by other authors (Chakrabarti 1989, 1996; Mukhopadhyay 2003). Other models were proposed by e.g. Gierliński et al. (1999), Coppi (1999), Zdziarski et al. (2001), including a secondary component in the accretion disc. On the other hand, Narayan & Yi (1995) introduced a two temperature disc model in the regime of inefficient cooling resulting in a vertical thickening of the hot disc gas. Here the pressure forces are expected to become important in modifying the disc dynamics which is likely to be sub-Keplerian. Other models with similar properties were proposed by, e.g., Begelman (1978), Liang & Thompson (1980), Rees et al. (1982), Eggum, Coroniti & Katz (1988). Abramowicz et al. (1988) proposed a height-integrated disc model, namely “slim disc”, having high optical depth of the accreting gas at super-Eddington accretion rate such that the diffusion time is longer than the viscous time. The model was further applied to study the thermal and viscous instabilities in optically thick accretion discs (Wallinder 1991; Chen & Taam 1993).

Shapiro, Lightman & Eardley (1976) initiated a two temperature Keplerian accretion disc at a low mass accretion rate which is optically thin and significantly hotter than the single temperature Keplerian disc of Shakura & Sunyaev (1973). The optically thin hot gas cools down through the bremsstrahlung and inverse-Compton processes and could explain various states of Cyg X-1 (Melia & Misra 1993). Similarly, the “ion torus” model by Rees et al. (1982) was applied to explain AGNs at a low mass accretion rate. However, the two temperature model solutions by Shapiro, Lightman & Eardley (1976) appear thermally unstable. Narayan & Popham (1993) and subsequently Narayan & Yi (1995) showed that introduction of advection may stabilize the system. However, the solutions of Narayan & Yi (1995), while of two temperatures, could explain only a particular class of hot systems with inefficient cooling mechanisms. They also described the hot flow based on the assumption of “self similarity” which is just a “plausible choice”. They kept the electron heating decoupled from the disc hydrodynamical computations which merely is an assumption. Later on, the solutions were attempted to generalize by Nakamura et al. (1997), Manmoto et al. (1997), Medvedev & Narayan (2001), relaxing efficiency of cooling into the systems, but concentrating only on specific classes of solutions. On the other hand, Chakrabarti & Titarchuk (1995) and later Mandal & Chakrabarti (2005) modeled two temperature accretion flows around Schwarzschild black holes in the general “advective paradigm”, emphasizing possible formation of shock and its consequences therein. However, they also did not include the effect of electron heating self-consistently into the hydrodynamical equation, and thus the hydrodynamical quantities do not get coupled to the rate of electron heating (see also Rajesh & Mukhopadhyay 2009).

In the present paper, we model a selfconsistent accretion flow in the regime of two temperature transonic sub-Keplerian disc (see also Sinha, Rajesh & Mukhopadhyay 2009; a brief version of the present work, but around Schwarzschild black holes). We consider all the hydrodynamical equations of the disc along with thermal components and solve the coupled set of equations selfconsistently. We neither restrict to the advection dominated regime nor the self-similar solutions. We allow the disc to cool selfconsistently according to the thermo-hydrodynamical evolution and compute the corresponding cooling efficiency factor as a function of radial coordinate. We investigate that when does the disc switch from the radiatively inefficient nature to general advective paradigm and vice versa.

In order to implement our model to explain observed sources, we focus on the under-luminous AGNs and quasars (e.g. Sgr A\*), ultra-luminous quasars and highly luminous AGNs (e.g. PKS 0743-67) and ultra-luminous X-ray (ULX) sources (e.g. SS433), when the last items are likely to be the “radiation trapped” accretion discs. While the first two cases correspond to respectively sub-Eddington and super-Eddington accretion flows around supermassive black holes, the last case corresponds to super-Eddington accretors around stellar mass black holes.

In the next section, we discuss the model equations describing the system and the procedure to solve them. Subsequently, we discuss the two temperature accretion disc flows around stellar mass and supermassive black holes, respectively in §3 and §4, for both sub-Eddington, Eddington and super-Eddington accretion rates. Section 5 compares the disc flow of low Shakura-Sunyaev (1973)  $\alpha$  with that of high  $\alpha$  and then between the flows around co and counter rotating black holes. Then we discuss the implications of the results with a summary in §6.

## 2 MODEL EQUATIONS DESCRIBING THE SYSTEM AND SOLUTION PROCEDURE

For the present purpose, we set five coupled differential equations describing the law of conservation in the sub-Keplerian optically thin accretion regime. Necessarily the set of equations describes the inner part of the accretion disc where the gravitational potential energy dominates over the centrifugal energy of the flow.

Throughout, we express all the variables in dimensionless units, unless stated otherwise. The radial velocity  $\vartheta$  and sound speed  $c_s$  are expressed in units of light speed  $c$ , the specific angular momentum  $\lambda$  in  $GM/c$ , where  $G$  is the Newton’s gravitational constant and  $M$  is the mass of the compact object, for the present purpose black hole, expressed in units of solar mass  $M_\odot$ , the radial coordinate  $x$  in units of  $GM/c^2$ , the density  $\rho$  and the total pressure  $P$  accordingly. The disc fluid under consideration consists of ions and electrons — thus two fluid/temperature system, apart from radiation. Furthermore, at the high temperature, the disc flow with ions/electrons behaves as (almost) noninteracting gas.

### 2.1 Conservation laws

(a) Mass transfer:

$$\frac{1}{x} \frac{\partial}{\partial x} (x\rho\vartheta) = 0, \quad (1)$$

whose integrated form gives the mass accretion rate

$$\dot{M} = -4\pi x \Sigma \vartheta, \quad (2)$$

where the surface density

$$\Sigma = I_n \rho h(x), \quad (3)$$

$$I_n = (2^n n!)^2 / (2n + 1)! \text{ (Matsumoto et al. 1984),} \quad (4)$$

$n$  is the polytropic index which is equal to  $1/(\gamma - 1)$  when  $\gamma$  is the ratio of specific heats, and half-thickness, based on the vertical equilibrium assumption, of the disc

$$h(x) = c_s x^{1/2} F^{-1/2}. \quad (5)$$

(b) Radial momentum balance:

$$\vartheta \frac{d\vartheta}{dx} + \frac{1}{\rho} \frac{dP}{dx} - \frac{\lambda^2}{x^3} + F = 0 \quad (6)$$

when following pseudo-Newtonian approach of Mukhopadhyay (2002)

$$F = \frac{(x^2 - 2a\sqrt{x} + a^2)^2}{x^3 [\sqrt{x}(x-2) + a]^2}, \quad (7)$$

where  $a$  is the specific angular momentum (Kerr parameter) of the black hole. We also define a parameter

$$\beta = \frac{\text{gas pressure } P_{gas}}{\text{total pressure } P} = \frac{6\gamma - 8}{3(\gamma - 1)} \text{ (e.g. Ghosh \& Mukhopadhyay 2009),} \quad (8)$$

where  $\gamma$  may range from  $4/3$  to  $5/3$ ,  $P_{gas} = P_i$  (ion pressure) +  $P_e$  (electron pressure), such that

$$P = \frac{\rho}{\beta c_s^2} \left( \frac{kT_i}{\mu_i m_i} + \frac{kT_e}{\mu_e m_i} \right) = \rho c_s^2, \quad (9)$$

where  $T_i$ ,  $T_e$  are respectively the ion and electron temperatures in Kelvin,  $m_i$  is the mass of proton in gm,  $\mu_i$  and  $\mu_e$  respectively are the corresponding effective molecular weight,  $k$  the Boltzmann constant. We assume  $\beta$  (and then  $\gamma$ ) constant throughout the flow.

(c) Azimuthal momentum balance:

$$\vartheta \frac{d\lambda}{dx} = \frac{1}{\Sigma x} \frac{d}{dx} (x^2 |W_{x\phi}|), \quad (10)$$

where following Mukhopadhyay & Ghosh (2003; hereinafter MG03) the shearing stress can be expressed in terms of the pressure and density as

$$W_{x\phi} = -\alpha (I_{n+1} P_{eq} + I_n \vartheta^2 \rho_{eq}) h(x), \quad (11)$$

where  $\alpha$  is the dimensionless viscosity parameter and  $P_{eq}$  and  $\rho_{eq}$  are the pressure and density respectively at the equatorial plane. Note that we will assume  $P_{eq} \sim P$  and  $\rho_{eq} \sim \rho$  in obtaining solutions.

(d) Energy production rate:

$$\frac{\vartheta h(x)}{\Gamma_3 - 1} \left( \frac{dP}{dx} - \Gamma_1 \frac{P}{\rho} \frac{d\rho}{dx} \right) = Q^+ - Q_{ie}, \quad (12)$$

where following MG03

$$Q^+ = \alpha (I_{n+1} P + I_n \vartheta^2 \rho) h(x) \frac{d\lambda}{dx}, \quad (13)$$

which is the heat generated by viscous dissipation, and  $Q_{ie}$  is the Coulomb coupling (Bisnovatyi-Kogan & Lovelace 2000) given in dimensional unit as

$$q_{ie} = \frac{8(2\pi)^{1/2} e^4 n_i n_e}{m_i m_e} \left( \frac{T_e}{m_e} + \frac{T_i}{m_i} \right)^{-3/2} \ln(\Lambda) (T_i - T_e) \text{ erg/cm}^3/\text{sec}$$

when  $q_{ie} = Q_{ie} c^{11} / (h G^4 M^3)$ . (14)

Here  $n_i$  and  $n_e$  denote number densities of ion and electron respectively,  $e$  the charge of an electron,  $\ln(\Lambda)$  the Coulomb logarithm. We also define (MG03)

$$\Gamma_3 = 1 + \frac{\Gamma_1 - \beta}{4 - 3\beta}, \quad (15)$$

$$\Gamma_1 = \beta + \frac{(4 - 3\beta)^2 (\gamma - 1)}{\beta + 12(\gamma - 1)(1 - \beta)}. \quad (16)$$

(e) Energy radiation rate:

$$\frac{\vartheta h(x)}{\Gamma_3 - 1} \left( \frac{dP_e}{dx} - \Gamma_1 \frac{P_e}{\rho} \frac{d\rho}{dx} \right) = Q_{ie} - Q^-, \quad (17)$$

where  $Q^-$  is the heat radiated away by the bremsstrahlung ( $q_{br}$ ), synchrotron ( $q_{syn}$ ) processes and inverse Comptonization ( $q_{comp}$ ) due to soft synchrotron photons, given in dimensionful form as

$$\bar{q}^- = q_{br} + q_{syn} + q_{comp}, \quad \text{when } \bar{q}^- = Q^- c^{11} / (h G^4 M^3). \quad (18)$$

Various components of the cooling processes may be read as (see Narayan & Yi 1995; Mandal & Chakrabarti 2005 for detailed description, what we do not repeat here)

$$\begin{aligned} q_{br} &= 1.4 \times 10^{-27} n_e n_i T_e^{1/2} (1 + 4.4 \times 10^{-10} T_e) \text{ erg/cm}^3/\text{sec}, \\ q_{syn} &= \frac{2\pi}{3c^2} k T_e \frac{v_a^3}{R} \text{ erg/cm}^3/\text{sec}, \quad R = x GM/c^2, \\ q_{comp} &= \mathcal{F} q_{syn}, \quad \mathcal{F} = \eta_1 \left( 1 - \left( \frac{x_a}{3\theta_e} \right)^{\eta_2} \right), \quad \eta_1 = \frac{p(A-1)}{(1-pA)}, \quad p = 1 - \exp(-\tau_{es}), \\ A &= 1 + 4\theta_e + 16\theta_e^2, \quad \theta_e = kT_e/m_e c^2, \quad \eta_2 = - \left( 1 + \frac{\ln(p)}{\ln(A)} \right), \quad x_a = h\nu_a/m_e c^2, \end{aligned} \quad (19)$$

where  $\tau_{es}$  is the scattering optical depth given by

$$\tau_{es} = \kappa_{es} \rho h \quad (20)$$

where  $\kappa_{es} = 0.38 \text{ cm}^2/\text{gm}$  and  $\nu_a$  is the synchrotron self-absorption cut off frequency determined by following Narayan & Yi (1995). Note that without a satisfactory knowledge of the magnetic field in accretion disks, following Mandal & Chakrabarti (1995), we assume the maximum possible magnetic energy density to be the gravitational energy density of the flow. As the total optical depth should include the effects of absorption due to nonthermal processes, effective optical depth is computed as

$$\tau_{\text{eff}} \approx \sqrt{\tau_{es} \tau_{abs}} \quad (21)$$

where

$$\tau_{abs} = \frac{h}{4\sigma T_e^4} (q_{br} + q_{syn} + q_{comp}) \frac{GM}{c^2}, \quad (22)$$

when  $\sigma$  is Stefan-Boltzmann constant.

Now combining all the above equations we obtain

$$\frac{d\vartheta}{dx} = \frac{N(x, \vartheta, c_s, \lambda, T_e)}{D(\vartheta, c_s)}, \quad (23)$$

where

$$\begin{aligned} N &= \frac{\Gamma_1 + 1}{\Gamma_3 - 1} \vartheta^2 c_s J - \frac{\alpha^2 c_s}{x} H \left( \frac{I_{n+1}}{I_n} c_s^2 + \vartheta^2 \right) - \alpha^2 \frac{I_{n+1}}{I_n} 2HJ + \frac{\Gamma_1 - 1}{\Gamma_3 - 1} \vartheta^2 c_s^3 L + \alpha H \left( \frac{2\lambda \vartheta c_s}{x^2} \right) \\ &\quad + \frac{4\pi Q_{ie}}{\dot{M}} \vartheta^2 c_s^2 x^{3/2} F^{-1/2}, \end{aligned} \quad (24)$$

$$D = \frac{1 - \Gamma_1}{\Gamma_3 - 1} c_s^3 \vartheta + 2\alpha c_s \frac{I_{n+1}}{I_n} H \left( \frac{c_s^2}{\vartheta} - \vartheta \right) + \frac{\Gamma_1 + 1}{\Gamma_3 - 1} \vartheta^2 c_s^2 \left( \vartheta - \frac{c_s^2}{\vartheta} \right) + \alpha^2 \vartheta H \left( \frac{H}{\vartheta} \right) \quad (25)$$

and

$$L = \left( \frac{3}{2x} - \frac{1}{2F} \frac{dF}{dx} \right), \quad H = (I_{n+1} c_s^2 + I_n \vartheta^2), \quad J = \left( c_s^2 L + \frac{\lambda^2}{x^3} - F \right). \quad (26)$$

We know that around the sonic radius  $N = D = 0$  (Mukhopadhyay 2003) and hence obtain the Mach number at this critical radius from  $D = 0$

$$M_c = \frac{\vartheta_c}{c_{sc}} = \sqrt{\frac{-B + (B^2 - 4AC)^{1/2}}{2A}}, \quad (27)$$

where

$$\begin{aligned} A &= \frac{\Gamma_1 + 1}{1 - \Gamma_3} - 2\alpha^2 (I_{n+1} - I_n), \quad B = \frac{2(\Gamma_1 + 1)}{1 - \Gamma_3} - 2\alpha^2 \frac{I_{n+1}}{I_n} (I_{n+1} - I_n), \\ C &= \alpha^2 \frac{I_{n+1}}{I_n} (1 - 2I_{n+1}). \end{aligned} \quad (28)$$

Also from  $N = 0$ , we can compute explicitly  $c_{sc}$  as a function of sonic/critical radius  $x_c$ . For a physical  $x_c$ , what one has to adjust in order to obtain a physical solution connecting outer boundary to black hole horizon through  $x_c$ ,  $c_{sc}$  and then  $\vartheta_c$  can be assigned, discussed in APPENDIX A in detail. Note that an improper  $x_c$  may lead to an unphysical/imaginary  $c_{sc}$  and  $\vartheta_c$ .

Finally combining Eqns. (6), (10) and (17) we obtain

$$\frac{dc_s}{dx} = \left( \frac{c_s}{\vartheta} - \frac{\vartheta}{c_s} \right) \frac{d\vartheta}{dx} + \frac{J}{c_s}, \quad (29)$$

$$\frac{d\lambda}{dx} = \left( \frac{2\alpha x}{\vartheta c_s} \frac{I_{n+1}}{I_n} \left( \frac{c_s^3}{\vartheta} - \vartheta c_s \right) + \alpha x \right) \frac{d\vartheta}{dx} + \left( \frac{c_s^2 - 2\alpha J}{c_s} + \vartheta \right), \quad (30)$$

$$\frac{dT_e}{dx} = (1 - \Gamma_1) T_e \frac{\vartheta}{c_s^2} \frac{d\vartheta}{dx} + (1 - \Gamma_1) T_e \left( \frac{J}{c_s^2} + L \right) + \frac{(\Gamma_3 - 1) 4\pi}{\dot{M}} \frac{c_s x^{3/2}}{F^{1/2}} (Q^{ie} - Q^-). \quad (31)$$

Hence knowing  $\vartheta$  we can obtain other variables  $c_s$ ,  $\lambda$ ,  $T_e$ . Note that  $d\vartheta/dx$  is indeterminate (of 0/0 form) at  $x_c$ . APPENDIX B discusses the procedure to obtain  $d\vartheta/dx$  at  $x_c$ .

As the entropy increases inwards in advective flows (e.g. Narayan & Yi 1994; Chakrabarti 1996; MG03), there is a possibility of convective instability and then corresponding transport, as proposed by Narayan & Yi (1994). Dynamical convective instability arises when the square of effective frequency

$$v_{\text{eff}}^2 = v_{\text{BV}}^2 + v_r^2 < 0 \quad (32)$$

such that  $v_{\text{BV}}$  is the Brunt-Väisälä frequency given by

$$v_{\text{BV}}^2 = -\frac{1}{\rho} \frac{dP}{dx} \frac{d}{dx} \ln \left( \frac{P^{1/\gamma}}{\rho} \right) \quad (33)$$

and  $v_r$  is the radial epicyclic frequency.

## 2.2 Solution procedure

In order to obtain the steady state solution, as of previous work (MG03, Mukhopadhyay 2003), primarily we need to fix the appropriate critical radius  $x_c$  (in fact the energy at the critical radius which is not conserved in the present cases) and the corresponding specific angular momentum  $\lambda_c$  of the flow. The detailed description of the procedure to obtain physically meaningful values of  $x_c$  and  $\lambda_c$ , to be determined iteratively, is given in APPENDIX A. As the flow is considered to be of two temperatures, at  $x_c$  an appropriate electron temperature  $T_{ec}$  also needs to be determined; also discussed in APPENDIX A. Note that one has to adjust the set of values  $x_c$ ,  $\lambda_c$ ,  $T_{ec}$  appropriately/iteratively to obtain self-consistent solution connecting outer boundary and black hole event horizon through  $x_c$ . Depending on the type of accreting system to model, we then have to specify the related inputs:  $\dot{M}$ ,  $M$ ,  $\gamma$  and  $a$ . Important point to note is that unlike former works (e.g. Chakrabarti & Titarchuk 1995, Chakrabarti 1996, MG03) here  $x_c$  changes with the change of  $\dot{M}$ , because the various cooling processes considered here explicitly depend on  $\dot{M}$ . Finally, we have to solve the Eqn. (23) from  $x_c$  to inwards — upto the black hole event horizon, and to outwards — upto the transition radius  $x_o$  where the disc deviates from the Keplerian to the sub-Keplerian regime such that  $\lambda/\lambda_K = 1$  ( $\lambda_K$  being the specific angular momentum of the Keplerian part of the disc). Figure 1 shows how the ratio  $\lambda/\lambda_K$  varies as a function of radial coordinate for different  $a$ . Note that higher  $a$ , which corresponds to a lower disc angular momentum (Mukhopadhyay 2003), reassembles the Keplerian part advancing with a smaller size of the sub-Keplerian disc. On the other hand, for a lower  $a$  the inner edge of the Keplerian component recedes. The fact of moving in and out of the inner edge of the disc reassembles respectively the soft and hard state of the black hole (e.g. Gilfanov et al. 1997). Hence it is naturally expected to link with the spin of the black hole.

However, the important point to note is that there is no selfconsistent model to describe the transition region where  $\lambda/\lambda_K = 1$ . Therefore, the transition of the flow from the Keplerian to sub-Keplerian regime does not appear smooth. This is mainly because the set of equations used to model the sub-Keplerian flow is not valid to explain the cold Keplerian flow, unless an extra boundary condition is imposed at the outer edge of the sub-Keplerian disc. However, in the present paper we do not intend to address the transition zone; rather we prefer to stick with the sub-Keplerian flow. Narayan et al. (1997) imposed boundary conditions at both the ends of accretion flows along with at the critical radius to fix the problem, at the cost of more input parameters than the parameters chosen in the present work. But still the transition of the flow from the Keplerian to sub-Keplerian regime remains undefined. Later Yuan (1999) discussed how the solutions vary with the change of outer boundary conditions influencing the structure of an optically thin accretion flow.

Below we discuss solutions in various parameter regimes to understand properties of the accretion disc around, first, stellar mass ( $M = 10$ ) and then super-massive ( $M = 10^7$ ) black holes.

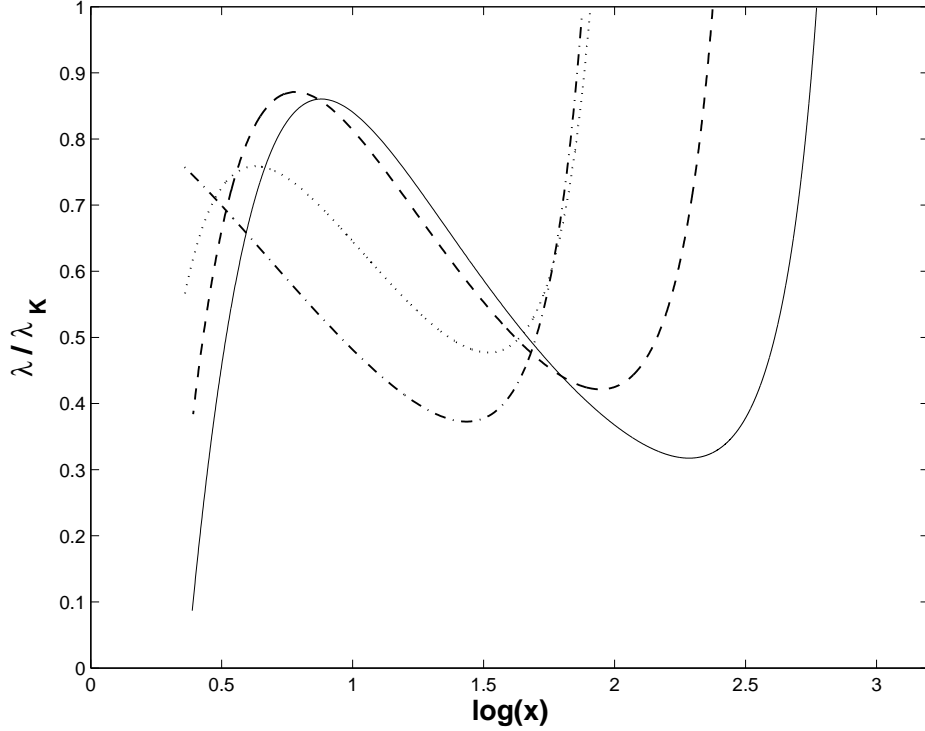


**Figure 1.** Variation of ratio of disc specific angular momentum to corresponding Keplerian angular momentum as a function of radial coordinate, when solid, dashed, dotted, dot-dashed lines correspond to the cases with  $a = -0.5, 0, 0.5, 0.998$  respectively. Other parameters are  $\dot{M} = 1$ ,  $M = 10$ ,  $\alpha = 0.01$ .

### 3 TWO TEMPERATURE ACCRETION DISC AROUND STELLAR MASS BLACK HOLES

Primarily we concentrate on two extreme regimes: (1) sub-Eddington and Eddington limits of accretion, (2) super-Eddington accretion. Furthermore, at each case of accretion rate, we focus on solutions around nonrotating (Schwarzschild) and rotating (Kerr with  $a = 0.998$ ) black holes.

One of our aims is to understand how the explicit cooling processes affect the disc dynamics and then the cooling efficiency vary over the disc radii. The cooling efficiency  $f$  is defined as the ratio of the energy advected by the flow to the energy dissipated, which is 1 for the advection dominated accretion flow (in short ADAF; Narayan & Yi 1994, 1995) and less than 1 for the general advective accretion flow (in short GAAF; Chakrabarti 1996; Mukhopadhyay 2003; MG03) in general. Therefore,  $f$  directly controls the ion and electron temperatures of the disc. Far away from the black hole where the gravitational power is weaker, the angular momentum profile becomes Keplerian and thus the disc becomes (or tends to become) of one temperature in the presence of efficient cooling.

#### 3.1 Sub-Eddington and Eddington accretors

##### 3.1.1 Schwarzschild black holes

We first consider flows around static black holes where the Kerr parameter  $a = 0$ . Figure 2 shows the behavior of flow variables as functions of radial coordinate for  $\dot{M} = 0.01, 0.1, 1$ ; throughout in the text we express  $\dot{M}$  in units of Eddington limit. The sets of input parameters for the model cases described here are given in Table 1. Figure 2a

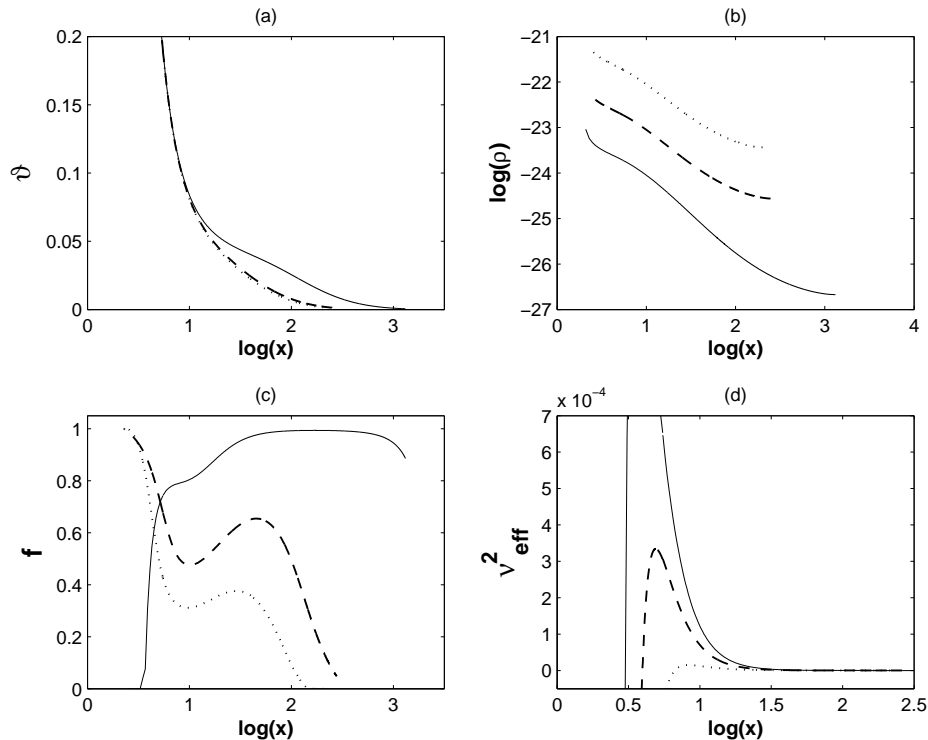


**Figure 2.** Variation of dimensionless (a) radial velocity, (b) density, (c) cooling factor, (d) square of convective frequency, as functions of radial coordinate for sub-Eddington and Eddington accretion flows. Solid, dashed, dotted curves are for  $\dot{M} = 0.01, 0.1, 1$  respectively. Other parameters are  $a = 0$ ,  $\alpha = 0.01$ ,  $M = 10$ ; see Table 1 for details.

Table 1: Parameters for accretion with  $\alpha = 0.01$  around black holes of  $M = 10$ , when the subscript ‘c’ indicates the quantity at the critical radius and  $T_{ec}$  is expressed in units of  $m_e c^2/k$

$\dot{M}$	$a$	$\gamma$	$x_c$	$\lambda_c$	$T_{ec}$
Sub-Eddington,			Eddington	accretors	
0.01	0	1.5	5.5	3.2	0.0001
0.01	0.998	1.5	3.5	1.7	0.0001
0.1	0	1.4	5.5	3.2	0.000164
0.1	0.998	1.4	3.5	1.7	0.000153
1	0	1.35	5.5	3.2	0.000225
1	0.998	1.35	3.5	1.7	0.0002122
Super-Eddington			accretors		
10	0	1.345	5.5	3.2	0.000181565
10	0.998	1.345	3.5	1.7	0.0004432
100	0	1.34	5.5	3.2	0.00038678
100	0.998	1.34	3.5	1.7	0.00055

verifies that a higher radial velocity corresponds to a lower mass accretion rate of the flow ( $\sim 0.01$ ) which results in less possible accumulation of matter in a particular radius attributing to a lower disc density (Fig. 2b). This hinders the bremsstrahlung process to cool the flow. However, at around  $x = 30$  the centrifugal barrier dominates and brings the velocity  $\vartheta$  down, particularly for  $\dot{M} = 0.01$ , which finally merges with that of higher  $\dot{M}$ -s. On the other hand, a lower  $\dot{M}$  corresponds to a gas dominated hot flow, which is radiatively less efficient and quasi-spherical in nature. As a result  $\vartheta$  is high, as seen in Fig. 2a. Efficiency of cooling is shown in Fig. 2c. Naturally a low  $\dot{M}$  corresponds to a radiatively inefficient flow rendering  $f \gtrsim 0.9$  upto  $x = 30$ . At  $x < 30$ , the dominance of centrifugal barrier slows down the infall which increases the residence time of matter in the disc before plunging into the black hole. This allows matter to have enough time to radiate by the synchrotron process and inverse Comptonization due to synchrotron soft photons, rendering  $f \rightarrow 0$  close to the black hole. In other words, for  $\dot{M} = 0.01$ , the disc is essentially radiatively inefficient, upto  $x \sim 30$ , and therefore the electron temperature never goes down. However, the density sharply increases in the vicinity of the black hole (Fig. 2b) which favors efficient cooling at a high temperature.

Therefore, although far away from the black hole a sub-Eddington flow appears to be radiatively inefficient, from  $x = 30$  onwards it



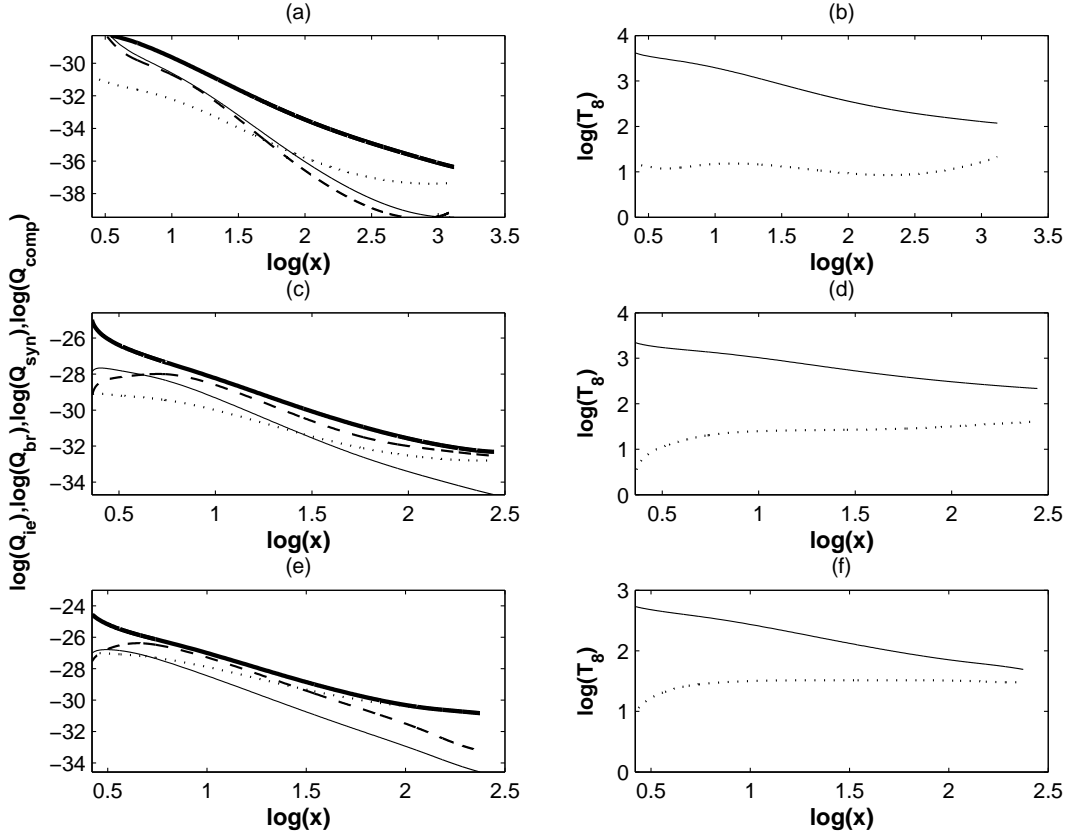


**Figure 3.** Variation of (a) dimensionless energy of Coulomb coupling (thicker line), bremsstrahlung (dotted line), synchrotron (solid), inverse Comptonization due to synchrotron photon (dashed line) processes in logarithmic scale, (b) corresponding ion (solid) and electron (dotted) temperatures in units of  $10^8\text{K}$ , as functions of radial coordinate for  $\dot{M} = 0.01$ . (c), (e) Same as (a) except  $\dot{M} = 0.1, 1$  respectively. (d), (f) Same as (b) except  $\dot{M} = 0.1, 1$  respectively. Other parameters are  $a = 0$ ,  $\alpha = 0.01$ ,  $M = 10$ ; see Table 1 for details.

turns out to be a radiatively efficient advective flow with  $f$  much less than unity. However, for  $\dot{M} = 0.1, 1$  the density is higher than that for  $\dot{M} = 0.01$  and hence the bremsstrahlung effect starts playing role in radiation mechanisms at much outer radii. This decreases the ion-electron temperature difference at the transition radius  $x_o$ . However, as the flow advances through the sub-Keplerian part, strong two temperature nature remains intact. For a higher  $\dot{M} (= 1)$ , however, the transition region is of marginally two temperatures. This is due to the efficient bremsstrahlung radiation at high density. In the vicinity of black hole  $T_e \sim 10^9\text{K}$  in the flow with  $\dot{M} = 0.01$  when  $f \rightarrow 0$ , as explained above, in the contrary to the cases with  $\dot{M} = 0.1, 1$  when  $f \rightarrow 1$  and  $T_e$  sharply decreases. Note that the accretion disc around a stellar mass black hole is arrested by significant magnetic field. This results in dominance of the synchrotron effect over the bremsstrahlung as the flow advances.

However, Fig. 2d shows that either of the cases do not exhibit convective instability (see, however, Narayan, Igumenshchev & Abramowicz 2000, Quataert & Gruzinov 2000) upto very inner edge, even if the radiatively inefficient flow deviates to a radiatively efficient GAAF. At a very inner edge, discs with  $\dot{M} = 0.1, 1$  particularly appear to be marginally unstable, which, although, seems not playing any role in angular momentum transfer.

Figure 3 describes how do the various cooling processes and corresponding temperature profiles vary as functions of radial coordinate. At a low  $\dot{M} (= 0.01)$  the system is radiatively inefficient, relative to that of higher  $\dot{M}$ -s ( $= 0.1, 1$ ), which brings out a hot two temperature Keplerian-sub-Keplerian transition region. As the flow advances through the sub-Keplerian part, strong two temperature nature remains intact. For a higher  $\dot{M} (= 1)$ , however, the transition region is of marginally two temperatures. This is due to the efficient bremsstrahlung radiation at high density. In the vicinity of black hole  $T_e \sim 10^9\text{K}$  in the flow with  $\dot{M} = 0.01$  when  $f \rightarrow 0$ , as explained above, in the contrary to the cases with  $\dot{M} = 0.1, 1$  when  $f \rightarrow 1$  and  $T_e$  sharply decreases. Note that the accretion disc around a stellar mass black hole is arrested by significant magnetic field. This results in dominance of the synchrotron effect over the bremsstrahlung as the flow advances.

### 3.1.2 Kerr black holes

We consider the rotating black holes with  $a = 0.998$ . As discussed earlier (Mukhopadhyay 2003), the angular momentum of the flow should be smaller around a rotating black hole compared to that around a static black hole. This reassembles advancing the Keplerian component which decreases size of the sub-Keplerian part. As the disc remains Keplerian (which is radiatively efficient) upto, e.g.,  $x \sim 100$  (see the



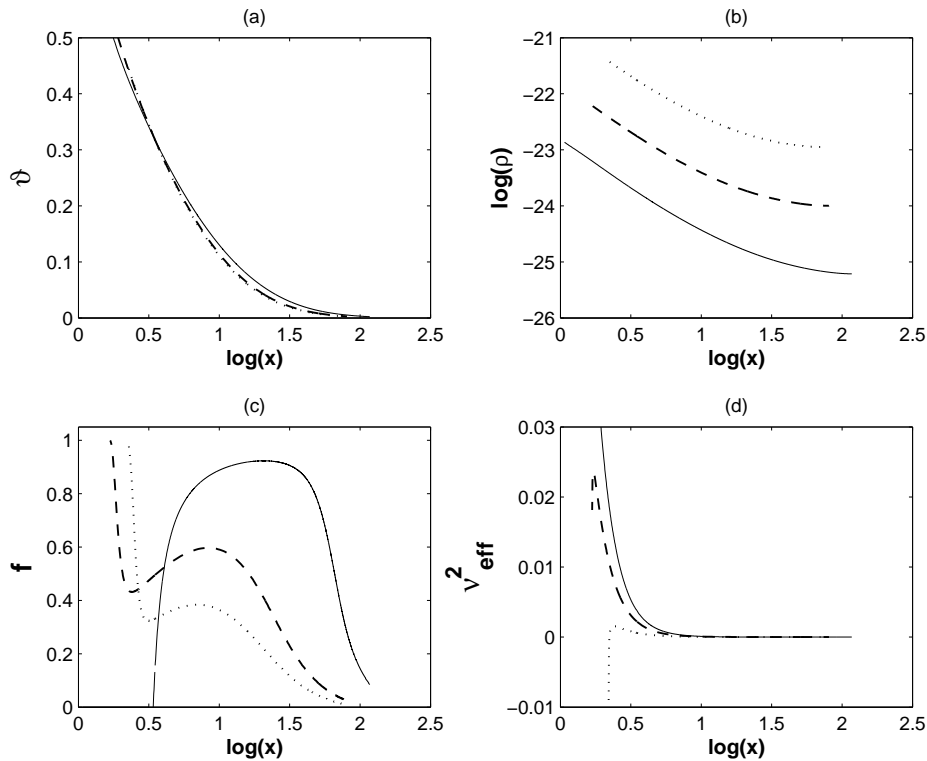


Figure 4. Same as Fig. 2, except  $a = 0.998$ .

outer radius in Fig. 4), the flow cools down significantly before deviating to the sub-Keplerian regime. Figure 4a shows that the velocity profiles for all  $\dot{M}$ -s are similar to each other, in absence of a strong centrifugal barrier. However,  $f$ , while very small at  $x \sim 100$ , increases as the sub-Keplerian flow advances. This is because the residence time of the flow decreases in an element of the sub-Keplerian disc hindering cooling processes to complete. Figure 4c shows that even  $f \rightarrow 0.9$  at  $x \sim 30$  for  $\dot{M} = 0.01$ , when the density is lowest (see Fig. 4b).

However, as the flow approaches to the black hole the synchrotron emission increases, and hence the system acquires enough soft photons which help in occurring the inverse Compton process. As a result the flow cools down further. When  $\dot{M} = 0.01$  the cooling process at the very inner edge of the accretion disc is dominant due to relatively high residence time of the flow, compared to that of a higher  $\dot{M}$ , rendering high  $T_e$  and then  $f \rightarrow 0$  very close to the black hole. Figure 4d proves that the flow is convectionally stable all the way upto the black hole event horizon. For  $\dot{M} \gtrsim 0.1$ , on the other hand, the flow is strongly advective and then unable to cool down before plunging into the black hole. Figure 5 shows the profiles of cooling processes and ion-electron temperatures. Basic nature of the profiles is pretty similar to that of Schwarzschild cases, except all of them advance in.

### 3.2 Super-Eddington accretors

The “radiation trapped” accretion disc can be attributed to the radiatively driven outflow or jet. This is likely to occur when the accretion rate is super-Eddington (Lovelace et al. 1994, Begelman et al. 2006, Fabbiano 2004, Ghosh & Mukhopadhyay 2009), as seen in the ultra luminous X-ray (ULX) sources such as SS433 (with luminosity  $\sim 10^{40}$  erg/s or so; Fabrika 2004). In order to describe such sources, the models described below are the meaningful candidates. We consider  $\dot{M} = 10, 100$ .

#### 3.2.1 Schwarzschild black holes

A high mass accretion rate significantly enhances density, upto two orders of magnitude compared to that of a low  $\dot{M}$ , which severely affects  $f$  and finally temperature profiles. The profiles of velocity shown in Fig. 6 are quite similar to that of sub-Eddington and Eddington cases. Because of similar reasons explained in §3.1.1 the profile exhibits a stronger centrifugal barrier for a lower  $\dot{M}$  ( $= 10$ ). A lower  $\dot{M}$  flow will have relatively more gas and then quasi-spherical structure compared to that of a higher  $\dot{M}$  ( $= 100$ ), which results in a lower velocity in the latter case. On the other hand, a lower velocity corresponds to a higher density which results in the strong bremsstrahlung radiation rendering  $f \rightarrow 0$ . For a lower  $\dot{M}$ , at  $x \sim 50$ , the energy radiated due to bremsstrahlung process becomes weaker than the energy transferred from protons to electrons through the Coulomb coupling (see Fig. 7), which increases  $f$  (see Fig. 6c). Subsequently, the synchrotron process becomes dominant (see Fig. 7), reassembling  $f \rightarrow 0$ . However, very close to the black hole a strong advection does not allow the flow,

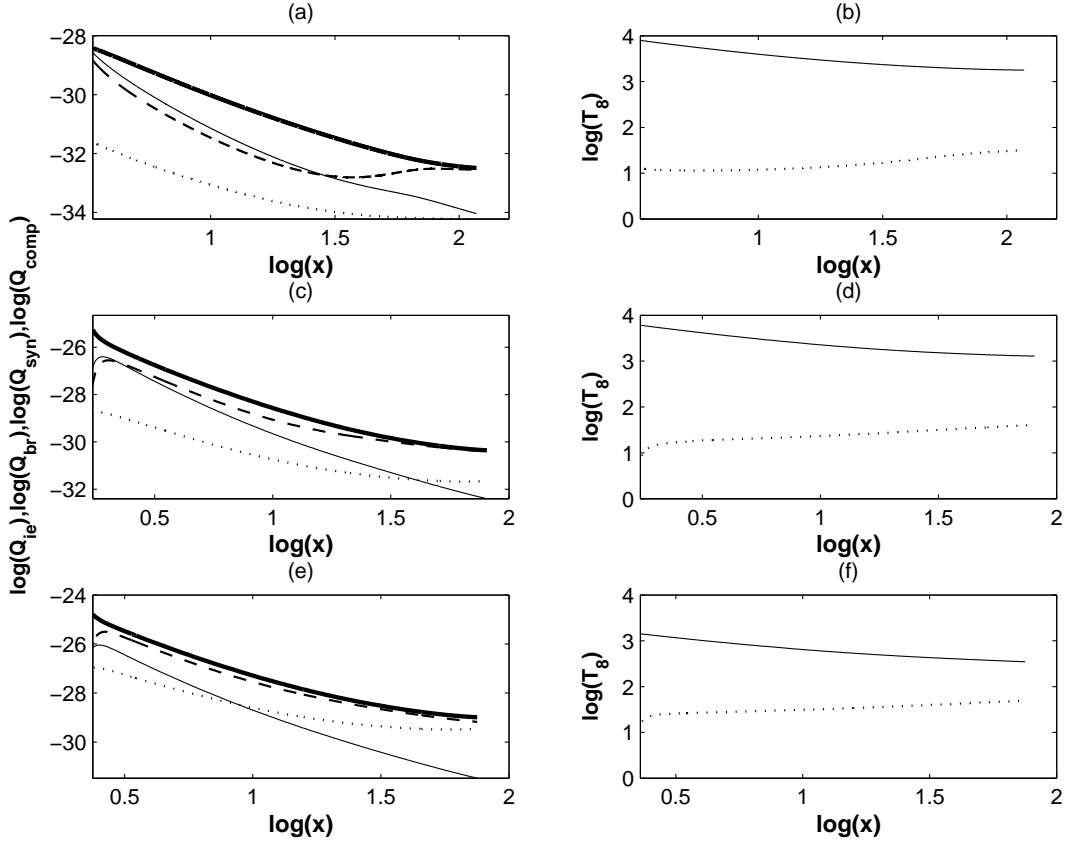


Figure 5. Same as Fig. 3, except  $a = 0.998$ .

independent of  $\dot{M}$ , to radiate efficiently rendering  $f \rightarrow 1$  again. This also results in marginal convective instability at  $x < 10$ , as shown in Fig. 6d.

Figure 7 shows that discs remain of one temperature at the transition radius. As the flows advance with a sub-Keplerian angular momentum,  $T_p$  profile deviates from that of  $T_e$ . For  $\dot{M} = 100$ , the high density flow is dominated by very efficient bremsstrahlung radiation all the way. In the vicinity of the black hole, an efficient cooling reassembles a sharp downfall of  $T_e$ .

### 3.2.2 Kerr black holes

As  $\lambda$  decreases in the case of a higher  $a$ , like low  $\dot{M}$  cases (see Mukhopadhyay 2003), the transition region advances an order of magnitude compared to that of Schwarzschild black holes. Similar to the cases of low  $\dot{M}$ , as shown in Fig. 8a, any centrifugal barrier smears out. However, unlike the flow around a static black hole, here the disc with  $\dot{M} = 10$  remains stable upto very close to the black hole. The reason is that a high  $a$  corresponds to a larger inner edge of the disc and thus the residence time of matter in the disc is higher. As a result the radiative processes keep cooling and then stabilizing the flow upto very inner edge.

Figure 9 shows that although a high  $\dot{M}$  exhibits a one temperature transition zone due to extremely efficient cooling processes, particularly due to bremsstrahlung radiation, as  $\dot{M}$  decreases the Keplerian disc itself becomes of two temperatures before deviating to the sub-Keplerian zone, unlike that of the Schwarzschild case. This is mainly because a flow with a high  $a$  brings the Keplerian disc further in where the transport of angular momentum increases leading to the decrease of the residence time of matter which does not allow an efficient cooling. However, the basic behaviours of various cooling processes is pretty similar to that around a static black hole.

## 4 TWO TEMPERATURE ACCRETION DISC AROUND SUPERMASSIVE BLACK HOLES

As of stellar mass black holes, here also we concentrate on two extreme regimes: (1) sub-Eddington and Eddington limits of accretion, (2) super-Eddington accretion; focusing on both nonrotating (Schwarzschild) and rotating (Kerr with  $a = 0.998$ ) black holes.

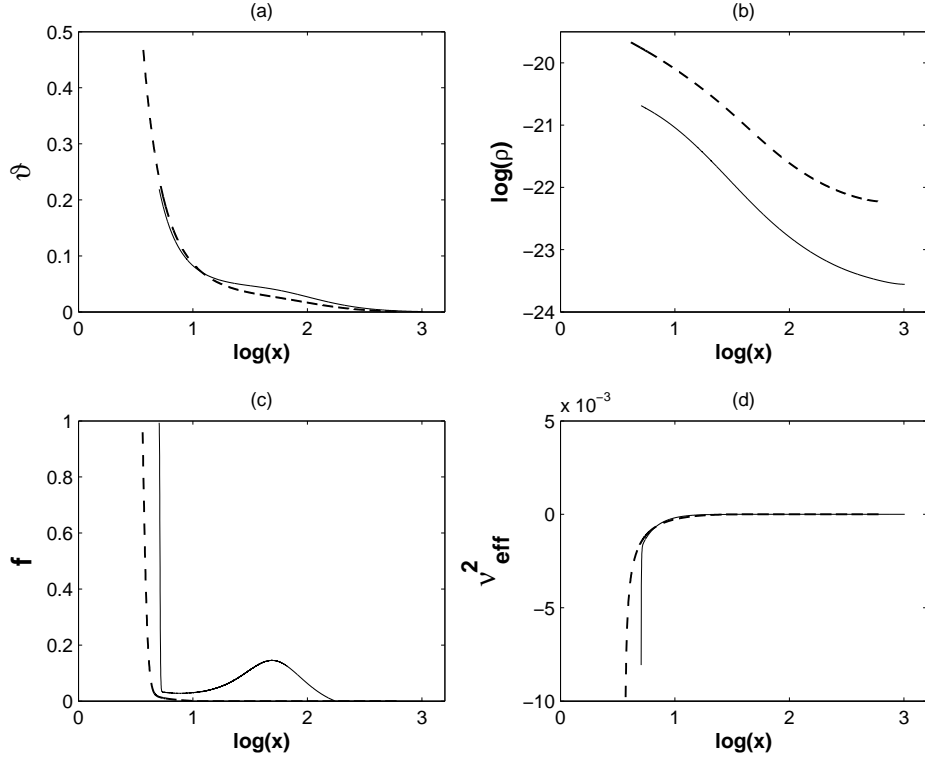


**Figure 6.** Variation of dimensionless (a) radial velocity, (b) density, (c) cooling factor, (d) square of convective frequency, as functions of radial coordinate for super-Eddington accretion flows. Solid, dashed curves are for  $\dot{M} = 10, 100$  respectively. Other parameters are  $a = 0$ ,  $\alpha = 0.01$ ,  $M = 10$ ; see Table 1 for details.

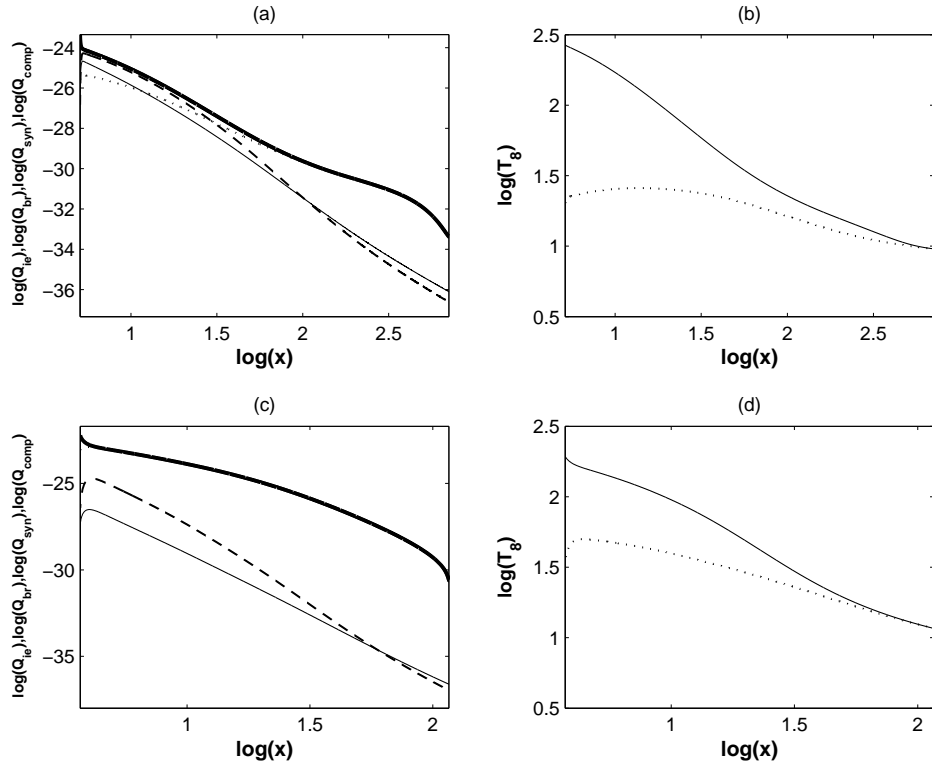


**Figure 7.** Variation of (a) dimensionless energy of Coulomb coupling (thicker line), bremsstrahlung (dotted line), synchrotron (solid), inverse Comptonization due to synchrotron photon (dashed line) processes in logarithmic scale, (b) corresponding ion (solid) and electron (dotted) temperatures in units of  $10^8 \text{K}$ , as functions of radial coordinate for  $\dot{M} = 10$ . (c) Same as (a) except  $\dot{M} = 100$ . (d) Same as (b) except  $\dot{M} = 100$ . Other parameters are  $a = 0$ ,  $\alpha = 0.01$ ,  $M = 10$ ; see Table 1 for details.

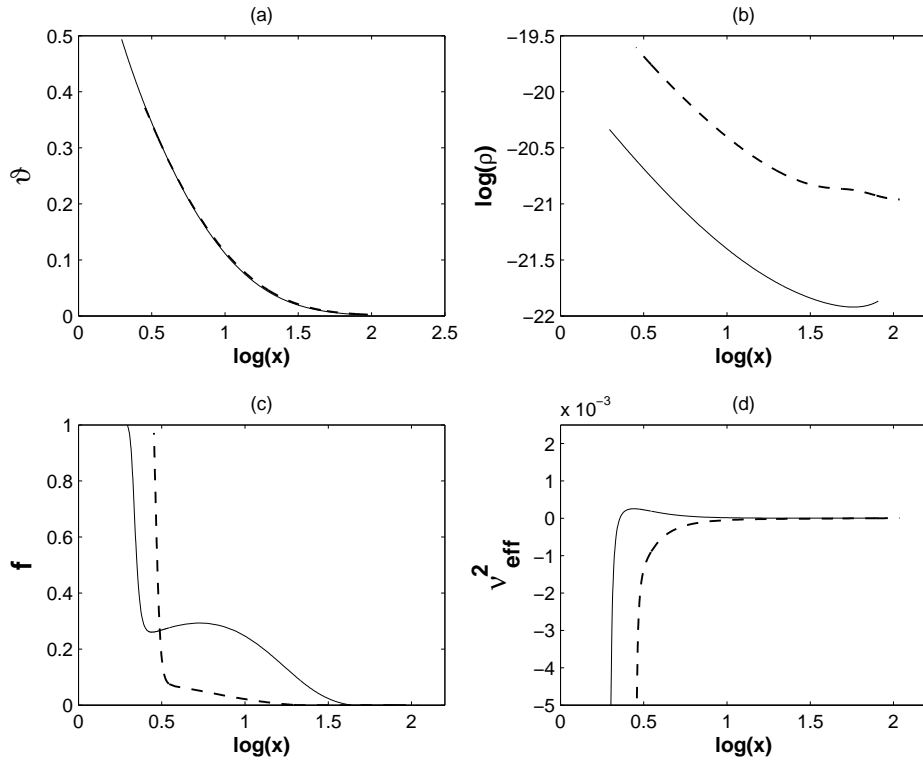


Figure 8. Same as Fig. 6, except  $a = 0.998$ .

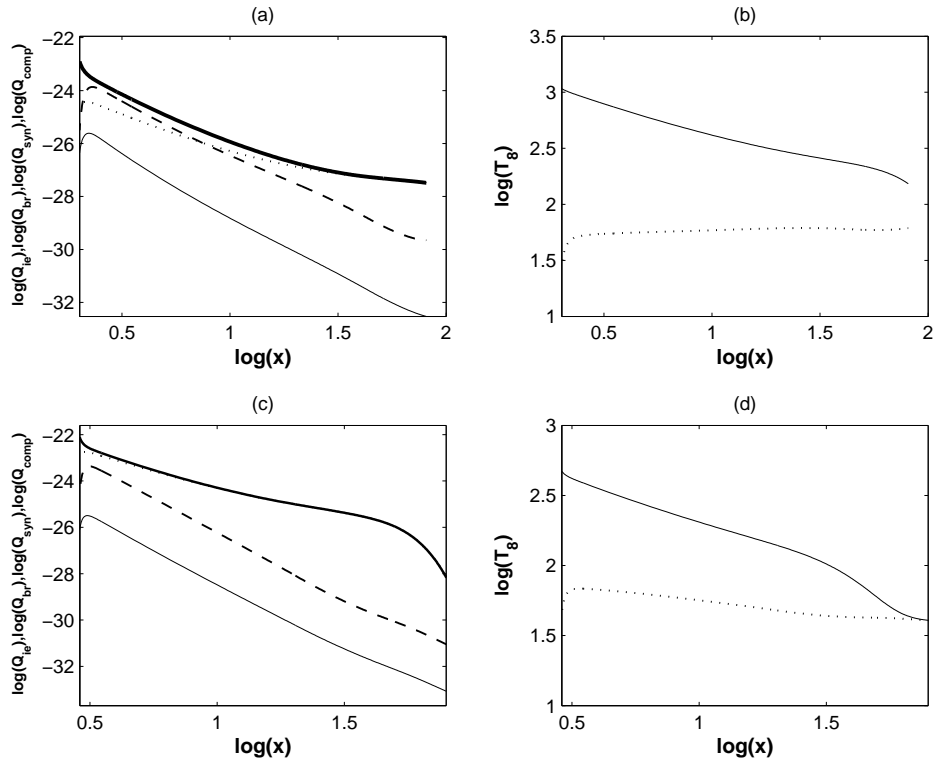
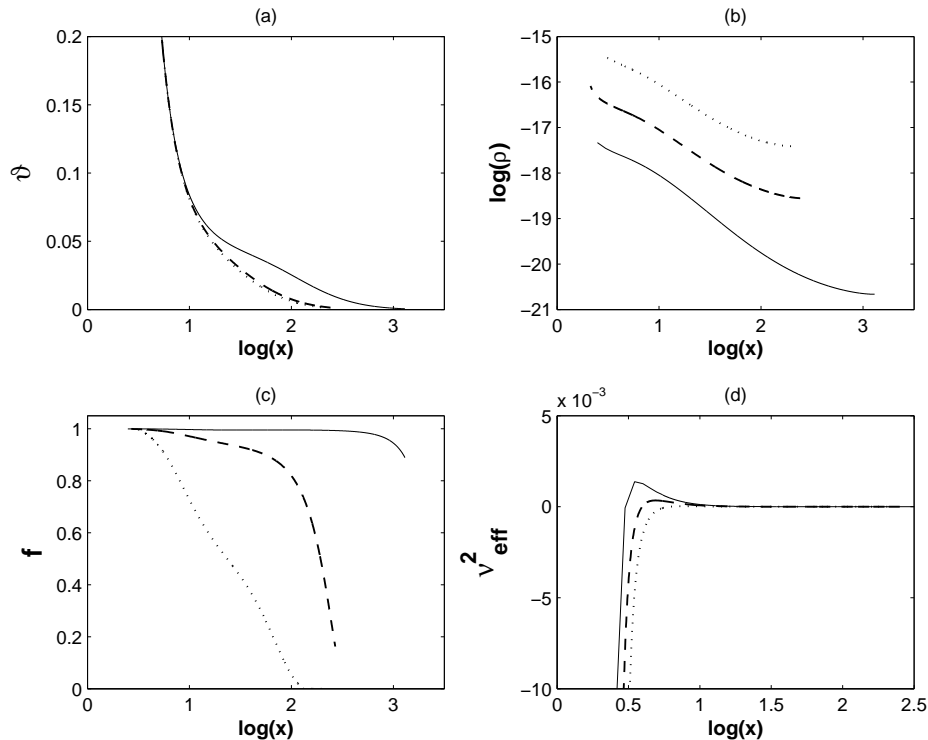


Figure 9. Same as Fig. 7, except  $a = 0.998$ .



**Figure 10.** Variation of dimensionless (a) radial velocity, (b) density, (c) cooling factor, (d) square of convective frequency, as functions of radial coordinate for sub-Eddington and Eddington accretion flows. Solid, dashed, dotted curves are for  $\dot{M} = 0.01, 0.1, 1$  respectively. Other parameters are  $a = 0$ ,  $\alpha = 0.01$ ,  $M = 10^7$ ; see Table 2 for details.

#### 4.1 Sub-Eddington and Eddington accretors

The under-luminous AGNs and quasars (e.g. Sgr A\*) had been already described by advection dominated model, where the flow is expected to be substantially sub-critical/sub-Eddington with a very low luminosity ( $\lesssim 10^{35}$  erg/s). Therefore the present cases, particularly of  $\dot{M} \leq 0.01$ , could be potential models in order to describe under-luminous sources.

##### 4.1.1 Schwarzschild black holes

Table 2 lists the sets of input parameters for the model cases described here. Naturally a disc around a supermassive black hole will have much lower density compared to that around a stellar mass black hole. Therefore, the cooling processes, particularly the bremsstrahlung radiation which is density dependent, are expected to be inefficient leading to a high  $f$ . However, the velocity profiles shown in Fig. 10a are very similar/same to that around a stellar mass black hole. Figure 10c shows that  $f \rightarrow 1$  in most of the sub-Keplerian regime for  $\dot{M} = 0.01$ . As  $\dot{M}$  increases, the density increases and thus the bremsstrahlung radiation increases, as shown in Fig. 11, which leads to the transition of radiatively inefficient flow to GAAF. When  $\dot{M} = 1$  the bremsstrahlung effect is very high resulting an GAAF with  $f$  much smaller than unity upto very close to the black hole. Figure 10d shows that close to the black hole there is a possible convective instability for all  $\dot{M}$ -s. This is because a strong advection of matter close to the black hole hindering cooling processes which results in  $f \rightarrow 1$ . This reassembles a possible convective instability at the inner edge. For a higher  $\dot{M}$ , the density is high which favours convection and thus brings the convective instability earlier in, at a relatively outer radius.

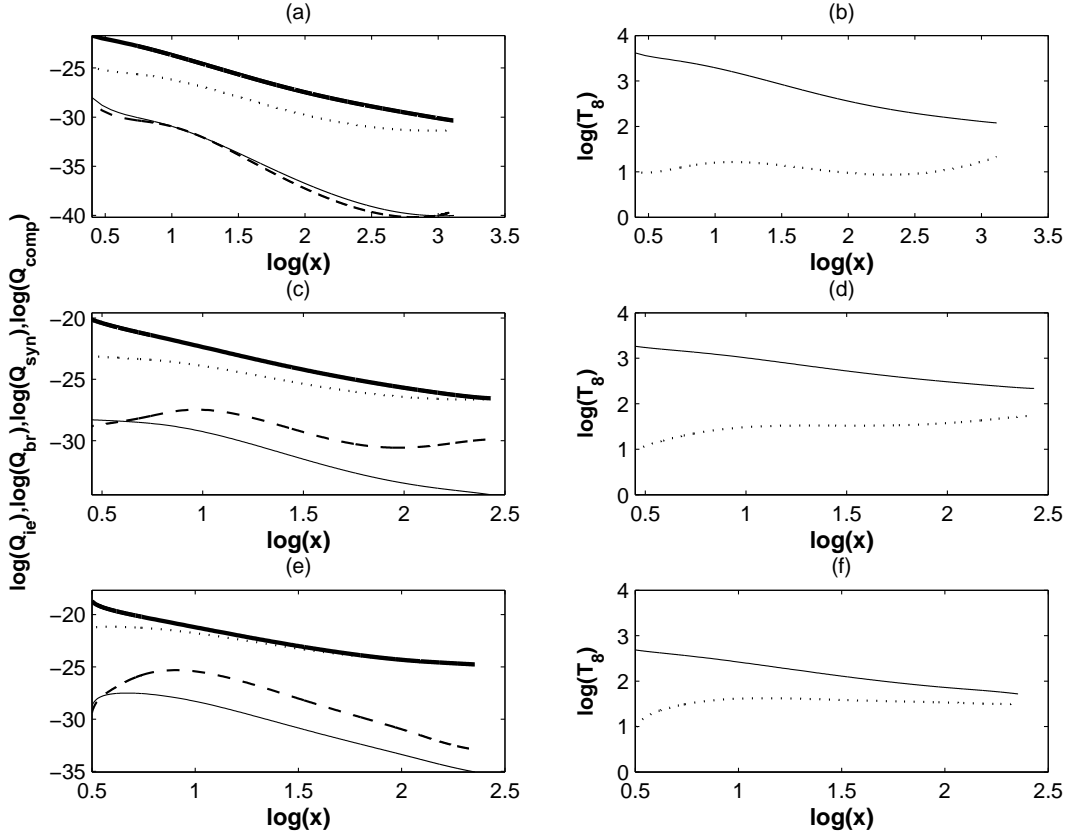


**Figure 11.** Variation of (a) dimensionless energy of Coulomb coupling (thicker line), bremsstrahlung (dotted line), synchrotron (solid), inverse Comptonization due to synchrotron photon (dashed line) processes in logarithmic scale, (b) corresponding ion (solid) and electron (dotted) temperatures in units of  $10^8\text{K}$ , as functions of radial coordinate for  $\dot{M} = 0.01$ . (c), (e) Same as (a) except  $\dot{M} = 0.1, 1$  respectively. (d), (f) Same as (b) except  $\dot{M} = 0.1, 1$  respectively. Other parameters are  $a = 0$ ,  $\alpha = 0.01$ ,  $M = 10^7$ ; see Table 2 for details.

Table 2: Parameters for accretion with  $\alpha = 0.01$  around black holes of  $M = 10^7$ , when the subscript ‘c’ indicates the quantity at the critical radius and  $T_{ec}$  is expressed in units of  $m_i c^2/k$

$\dot{M}$	$a$	$\gamma$	$x_c$	$\lambda_c$	$T_{ec}$
Sub-Eddington,			Eddington	accretors	
0.01	0	1.5	5.5	3.2	0.0001
0.01	0.998	1.5	3.5	1.7	0.0001
0.1	0	1.4	5.5	3.2	0.000178
0.1	0.998	1.4	3.5	1.7	0.00023
1	0	1.35	5.5	3.2	0.0002493
1	0.998	1.35	3.5	1.7	0.000295
Super-Eddington			accretors		
10	0	1.345	5.5	3.2	0.000427
10	0.998	1.345	3.5	1.7	0.0006
100	0	1.34	5.5	3.2	0.0003874
100	0.998	1.34	3.5	1.7	0.00059

The temperature profiles shown in Fig. 11 are pretty similar to what we obtain in stellar mass black holes what we do not explain here again. However, note that unlike stellar mass black holes, only the bremsstrahlung radiation is effective in cooling the flow around a supermassive black hole, particularly for  $\dot{M} = 1$ .

#### 4.1.2 Kerr black holes

The specific angular momentum of the black hole is chosen to be  $a = 0.998$ . The basic hydrodynamical properties are similar to that in Schwarzschild cases, except, like the flows around stellar mass black holes, the transition region advances due to a smaller angular momentum

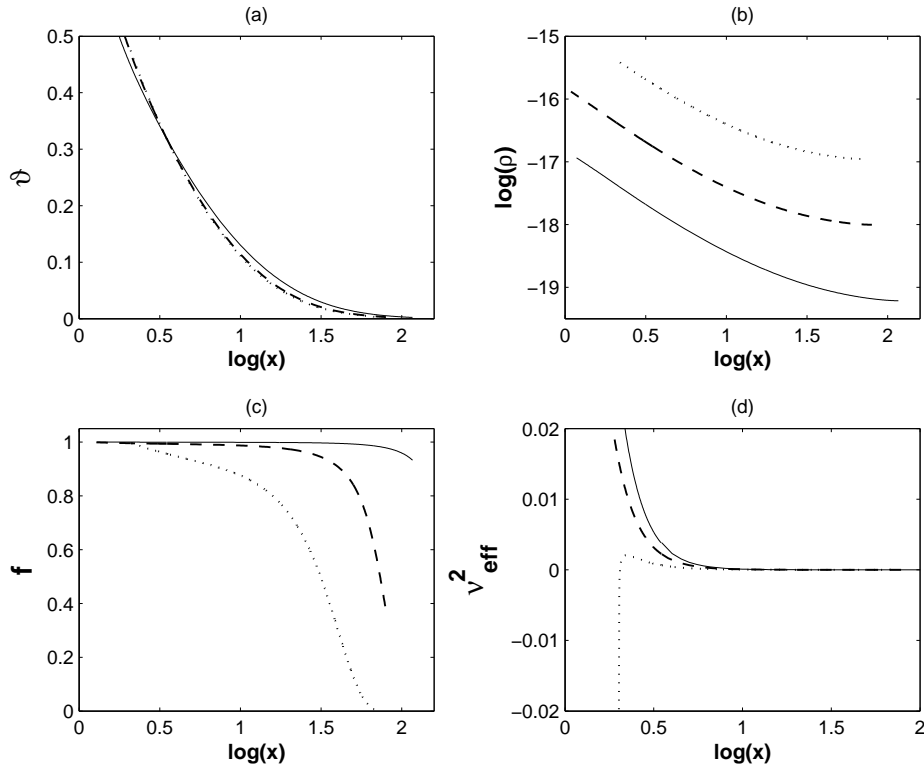


Figure 12. Same as Fig. 10, except  $a = 0.998$ .

of the flow, shown in Fig. 12. As discussed in §3.2.2, a higher  $a$  corresponds to a smaller  $\lambda$  which in turn decreases  $\vartheta$  at a particular radius of the inner edge of the disc, when the inner edge is stretched in, compared to that around a Schwarzschild black hole. This results in the increase of residence time of the flow in the sub-Keplerian disc before plunging into the black hole. Therefore, the bremsstrahlung process keeps cooling and then stabilizing the flow upto very inner edge. Important point to note, as a consequence, is that the disc flow around a rotating black hole is convectively more stable compared to that around a nonrotating black hole. This is particularly because the density gradient of the inner (e.g. the vicinity of  $x = 2$ , which is the event horizon for a nonrotating black hole) flow around a rotating black hole is less steeper compared to that around a nonrotating black hole, and hence the flow is convectively more stable in the former case.

Figure 13 shows that basic features of the temperature profiles are similar to the cases of static black holes. However, the transition region reveals that for a lower  $\dot{M}$ , the Keplerian flow exhibits the inverse Comptonization via synchrotron photons. As the flow advances with a sub-Keplerian angular momentum, the residence time decreases and thus inverse Comptonization decreases, resulting a hotter flow.

## 4.2 Super-Eddington accretors

Ultra-luminous accretors with a high kinetic luminosity ( $\sim 10^{46} - 10^{49}$  erg/s) radio jet have been observed in the highly luminous AGNs and ultra-luminous quasars (e.g. PKS 0743-67; Punnsly & Tingay 2005), possibly in ULIRs (Genzel et al. 1998) and narrow-line Seyfert 1 galaxies (e.g. Mineshige et al. 2000). Therefore, the following cases could be potential models to explain such sources.

### 4.2.1 Schwarzschild black holes

Figures 14 and 15 show that the basic flow properties are pretty similar to that around stellar mass black holes, except in the present cases the centrifugal barrier smears out. This is because a high black hole mass corresponds to a low density of the flow and thus a fast infall. This also results, unlike stellar mass black holes, in an inefficient synchrotron radiation even at the inner edge of the disc.

### 4.2.2 Kerr black holes

Figures 16 and 17 repeat the same story of that around stellar mass black holes, but with the smeared centrifugal barrier, as described above for static black holes. However, due to decreasing density, the overall cooling effects decrease keeping the disc hotter, particularly for  $\dot{M} = 10$ .



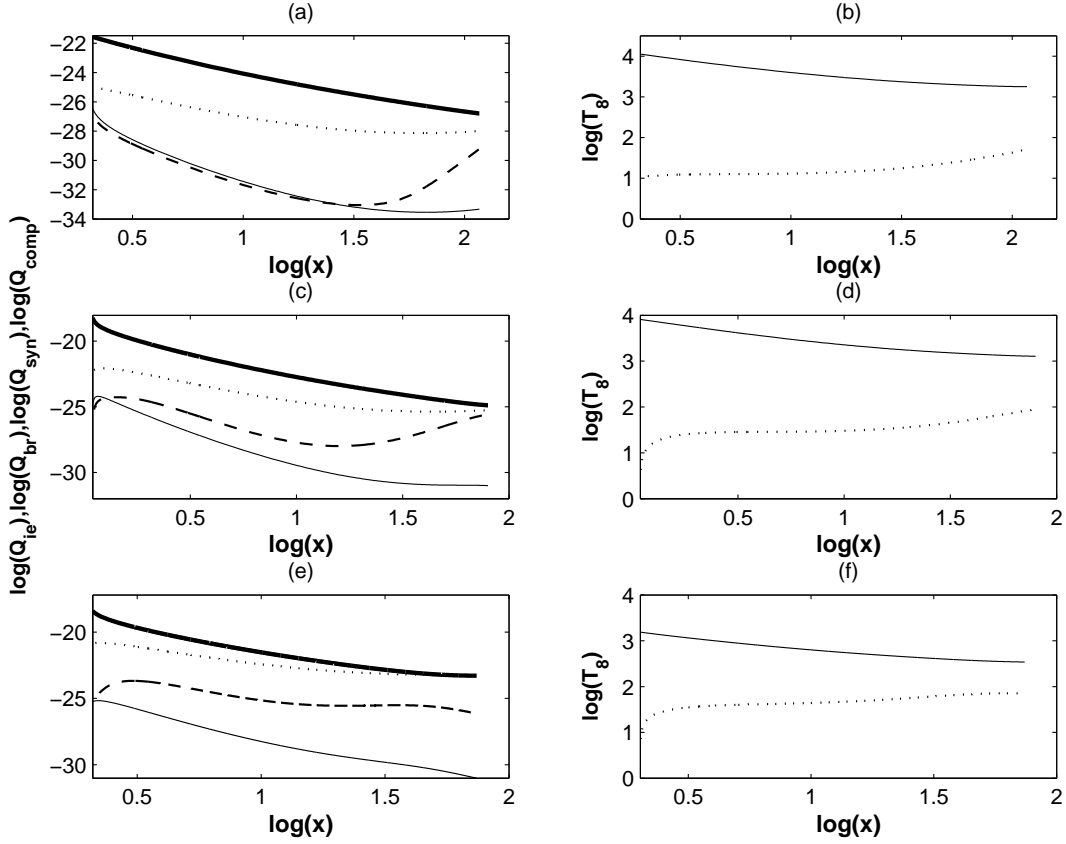


Figure 13. Same as Fig. 11, except  $\alpha = 0.998$ .

## 5 COMPARISON BETWEEN FLOWS WITH DIFFERENT $\alpha$ AND AROUND COROTATING AND COUNTER ROTATING BLACK HOLES

So far we have restricted to a typical Shakura-Sunyaev viscosity parameter  $\alpha = 0.01$ , for corotating black holes. Now we plan to explore a lower  $\alpha$ , as well as a counter rotating black hole to understand any significant change in the flow behaviour.

### 5.1 Comparison between flows with $\alpha = 0.01$ and $\alpha = 0.0001$

Decreasing  $\alpha$  naturally decreases the rate of energy-momentum transfer between any two successive layers of the fluid element and increasing the residence time of the flow in the sub-Keplerian disc. This also recedes the Keplerian-sub-Keplerian transition region further out. This is mainly because a low value of  $\alpha$  can not keep continuing the outward angular momentum transport efficiently in the Keplerian flow below a certain radial coordinate. Therefore, the disc flow can not remain Keplerian and becomes sub-Keplerian at a larger radius, compared to a flow of high  $\alpha$ .

We know, on the other hand, that increasing residence time increases the possibility of completing various radiative processes in the disc flow, before the infalling matter plunges into the black hole. Therefore, the flow is expected to appear cooler with smaller  $f$ . Hence, for the purpose of comparison, we consider a flow with  $\dot{M} = 0.01$  around a supermassive black hole of  $M = 10^7$ , e.g. Sgr A\*, which is radiatively inefficient and hot for  $\alpha = 0.01$ .

Figure 18 shows that although the velocity profiles are similar for both the values of  $\alpha$ , the size of the sub-Keplerian disc is about five times for  $\alpha = 0.0001$  than that for  $\alpha = 0.01$ . Inside  $x = 17$  the low  $\alpha$  disc flow becomes cooler very fast, rendering  $f \rightarrow 0$  at  $x > 10$  (see Fig. 18c). Therefore, the flow sharply transits from radiatively inefficient in nature to GAAP. As a consequence, the low  $\alpha$  flow remains stable, as shown in Fig. 18b, all the way upto the event horizon. As the sub-Keplerian flow of a smaller  $\alpha$  extends further away where the influence of black hole is very weak,  $T_e$  and  $T_i$  merge (see Fig. 18d) before the flow crosses the transition radius, unlike the flow with  $\alpha = 0.01$  when  $T_i > T_e$  there.

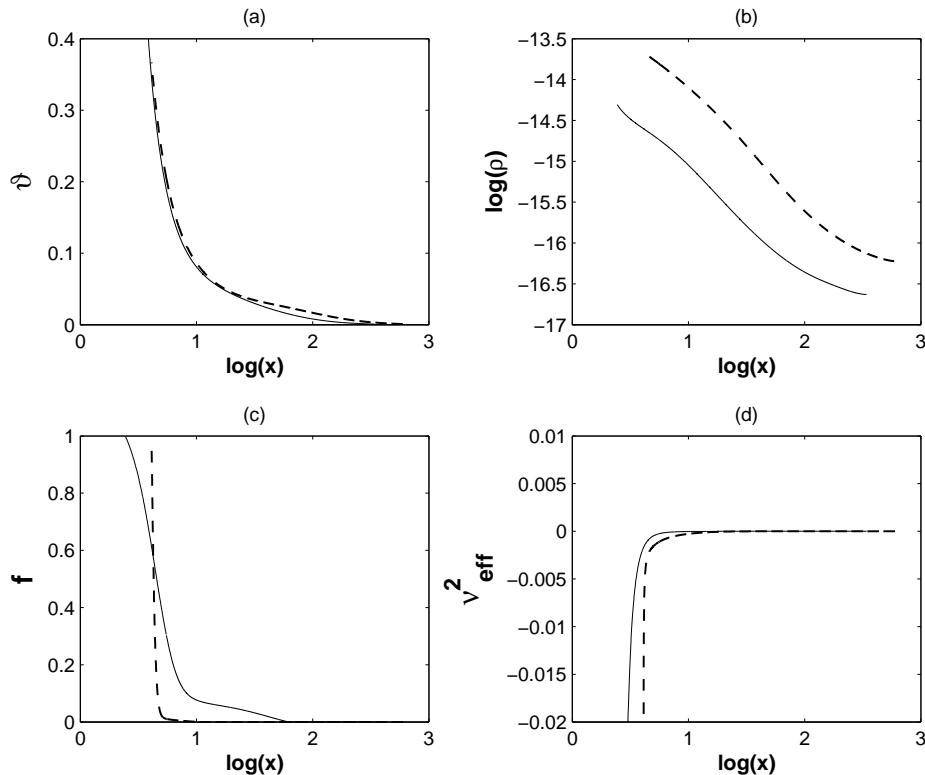


**Figure 14.** Variation of dimensionless (a) radial velocity, (b) density, (c) cooling factor, (d) square of convective frequency, as functions of radial coordinate for super-Eddington accretion flows. Solid, dashed curves are for  $\dot{M} = 10, 100$  respectively. Other parameters are  $a = 0$ ,  $\alpha = 0.01$ ,  $M = 10^7$ ; see Table 2 for details.

## 5.2 Comparison between flows around co and counter rotating black holes

As we already discussed that the model with a low mass accretion rate around a supermassive black hole is a potential case in explaining the observed dim source Sgr A\*. On the other hand, the ultra-luminous X-ray sources presumably correspond to the models with a high mass accretion flow around a stellar mass black hole. Therefore, in order to compare the flow properties between co and counter rotating black holes, we choose these two extreme cases.

Qualitatively, the flows with similar initial conditions around co and counter rotating black holes of same mass are similar, as shown in Figs. 19, 20 for  $a = \pm 0.5$ . However, the sub-Keplerian disc size around the black hole with  $a = -0.5$  is smaller due to smaller value of the effective angular momentum (Mukhopadhyay 2003) of the system. Hence the radial velocity is almost an order of magnitude higher, particularly at the inner edge, for  $a = -0.5$ .

## 6 DISCUSSION AND SUMMARY

We model the two temperature accretion flow, particularly around black holes, combining the equations of conservation and comprehensive cooling processes. We consider self-consistently the important cooling mechanisms: bremsstrahlung, synchrotron and inverse Comptonization due to synchrotron photons, where ions and electrons are allowed to have different temperatures. As matter falls in, hot electrons cool through the various cooling mechanisms, particularly by the synchrotron emission when the magnetic field is high. This is particularly the case for the flow around stellar mass black holes where the magnetic field may also act as a boost in transporting the angular momentum. However, in the present paper, we do not consider such processes in detail, rather stick with the standard  $\alpha$ -prescription.

By solving a complete set of disc equations we show that in general the disc system exhibits GAUF. However, in certain circumstances GAUF becomes radiatively inefficient, depending on the flow parameters and hence efficiency of cooling mechanisms. Transitions from GAUF to radiatively inefficient flow and vice versa are clearly explained by the cooling efficiency factor  $f$ , shown in each model cases. While the previous authors, who proposed ADAF (Narayan & Yi 1994, 1995), especially restricted with flows having  $f = 1$  (inefficient cooling), here we do not impose any restriction to the flow parameters to start with and let the parameter  $f$  to determine self-consistently as the system evolves. Therefore, our model is very general whose special case may be understood as a radiatively inefficient advection dominated flow.

We have explored especially the optically thin flows incorporating bremsstrahlung, synchrotron and inverse Comptonization processes. In Fig. 21 we show the variation of the effective optical depth as a function of disc radii for two limiting cases. While flows around rotating

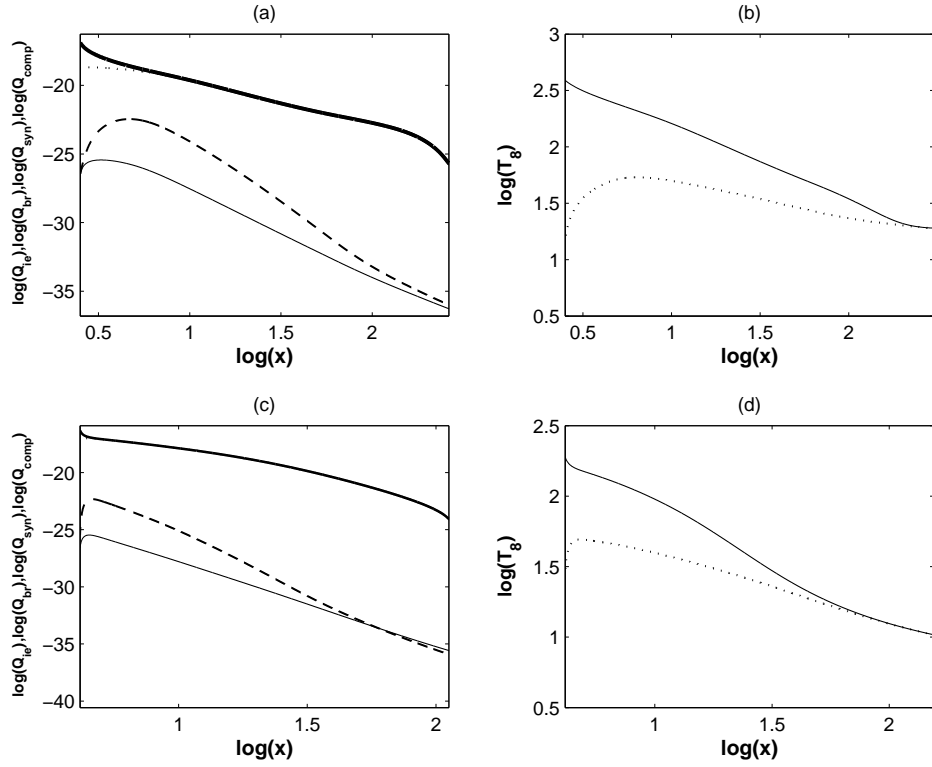


**Figure 15.** Variation of (a) dimensionless energy of Coulomb coupling (thicker line), bremsstrahlung (dotted line), synchrotron (solid), inverse Comptonization due to synchrotron photon (dashed line) processes in logarithmic scale, (b) corresponding ion (solid) and electron (dotted) temperatures in units of  $10^8 \text{K}$ , as functions of radial coordinate for  $\dot{M} = 10$ . (c) Same as (a) except  $\dot{M} = 100$ . (d) Same as (b) except  $\dot{M} = 100$ . Other parameters are  $a = 0$ ,  $\alpha = 0.01$ ,  $M = 10^7$ ; see Table 2 for details.

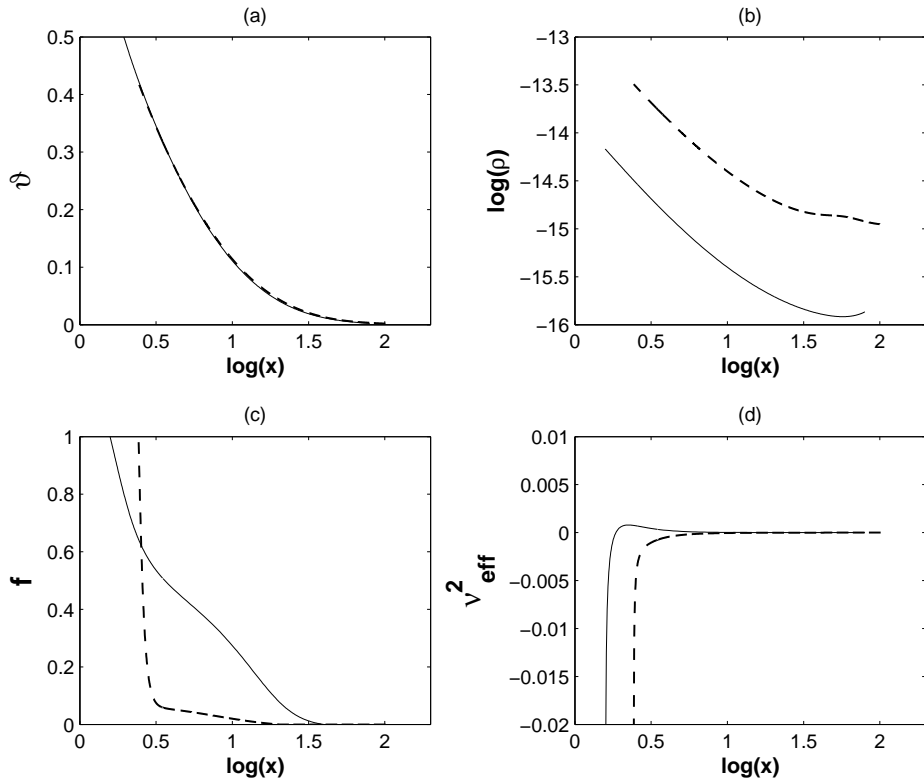


**Figure 16.** Same as Fig. 14, except  $a = 0.998$ .

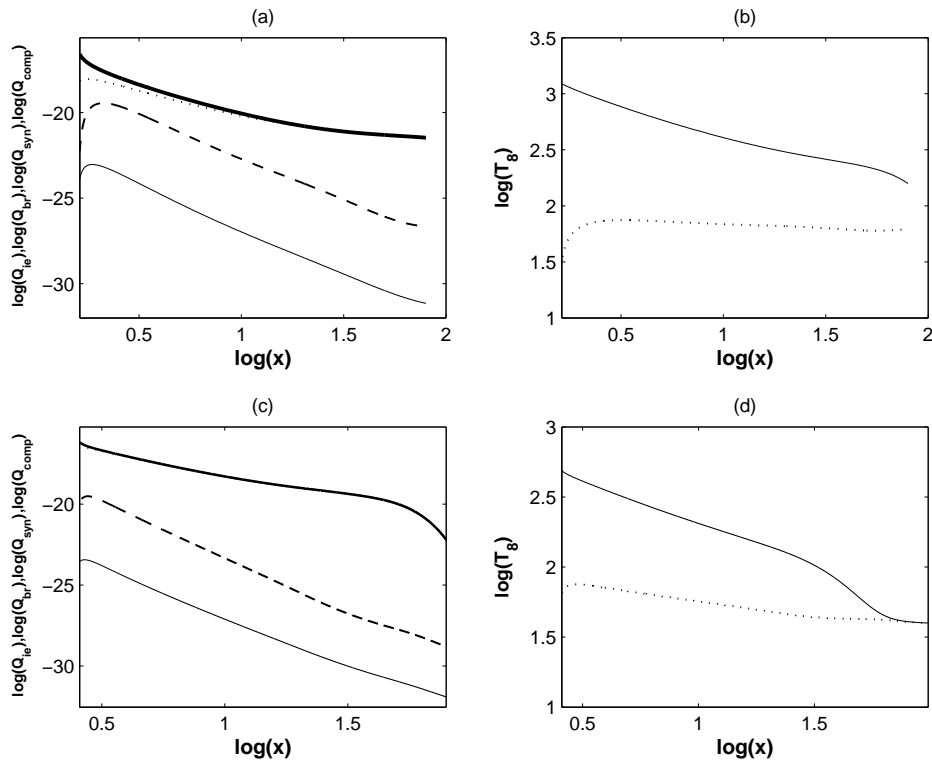


Figure 17. Same as Fig. 15, except  $a = 0.998$ .

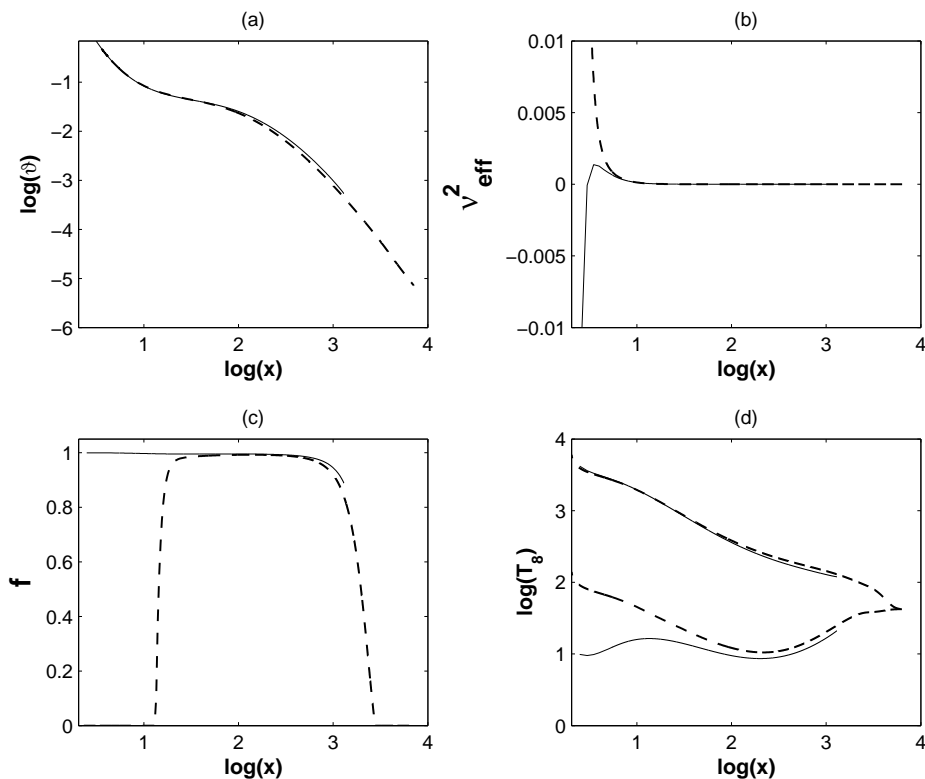
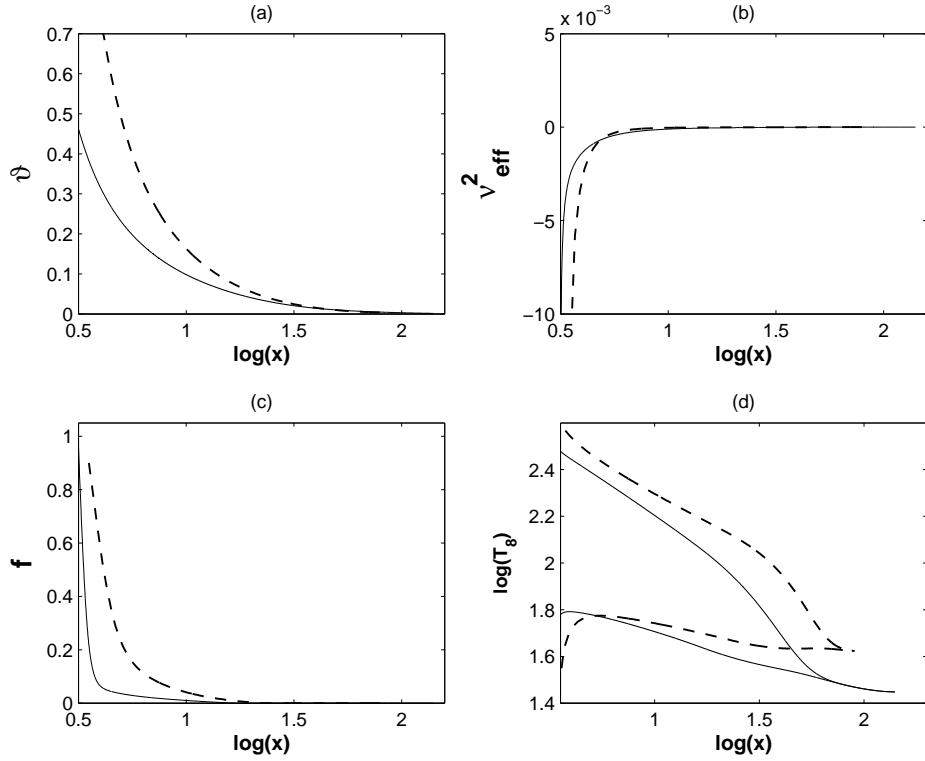
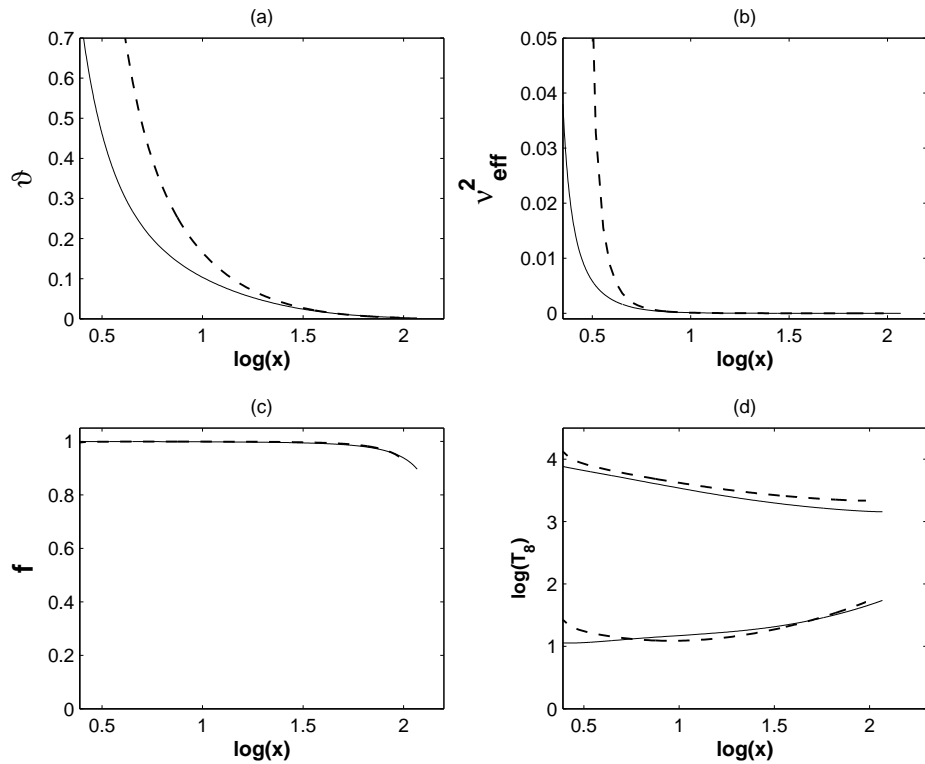


Figure 18. Comparison between solutions for high and low  $\alpha$ : Variation of (a) velocity, (b) square of convective frequency, (c) cooling factor, (d) ion (upper set of lines) and electron (lower set of lines) temperatures, a functions of radial coordinate, when solid lines correspond to  $\alpha = 0.01$  and dashed lines correspond to  $\alpha = 0.0001$ . Other parameters are  $\dot{M} = 0.01$ ,  $M = 10^7$ ,  $a = 0$ .



**Figure 19.** Comparison between solutions for co and counter rotating stellar mass black holes: Variation of (a) velocity, (b) square of convective frequency, (c) cooling factor, (d) ion (upper set of lines) and electron (lower set of lines) temperatures, as functions of radial coordinate, when solid lines correspond to  $b = 0.5$  and dashed lines correspond to  $b = -0.5$ . Other parameters are  $\dot{M} = 100$ ,  $M = 10$ ,  $\alpha = 0.01$ .



**Figure 20.** Same as Fig. 19, except  $\dot{M} = 0.01$ ,  $M = 10^7$ .

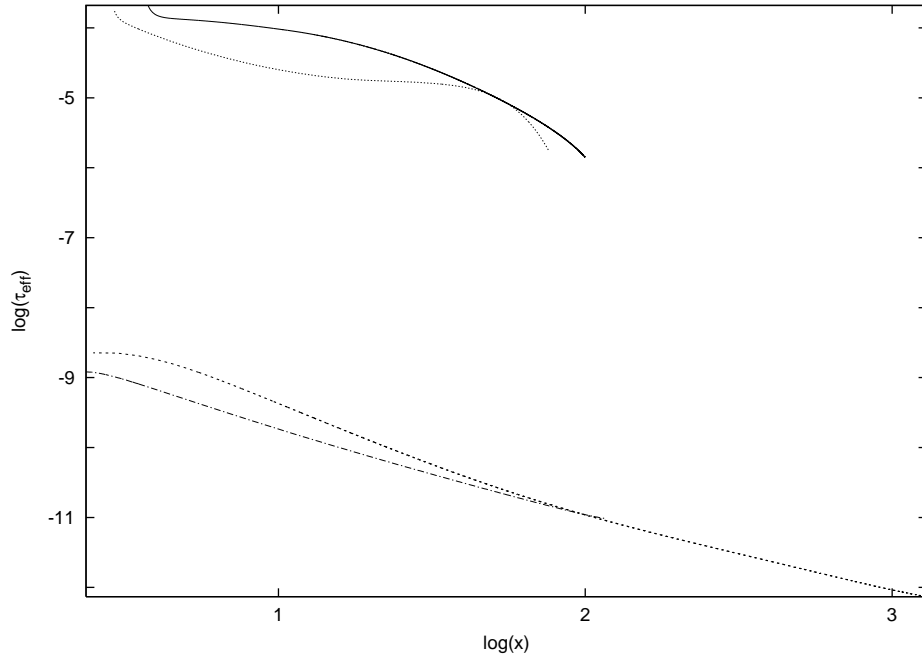


**Figure 21.** Variation of the effective optical depth as a function of radial coordinate. Solid ( $a = 0$ ) and dotted ( $a = 0.998$ ) curves correspond to  $M = 10$ ,  $\dot{M} = 100$  and dashed ( $a = 0$ ) and dot-dashed ( $a = 0.998$ ) curves correspond to  $M = 10^7$ ,  $\dot{M} = 0.01$ . See Tables 1 and 2 for details.

black holes appear slightly thinner compared to the corresponding cases of static black holes, in general  $\tau_{\text{eff}} \lesssim 5 \times 10^{-4}$ . This verifies our choice of optically thin flows throughout. However, for the present purpose, when the main aim is to understand disk dynamics in the global, viscous, two-temperature regime, we have ignored inverse Comptonization due to bremsstrahlung photons, if any. This may be important in cases of very super-Eddington accretion flows which we plan to explore in future, particularly, in analysing the underlying spectra.

The temperature of the flow depends on the accretion rate. If the accretion rate is low and thus the flow is radiatively inefficient, then the disc is hot. Such a hot flow is being attempted to model since 1976 (Shapiro, Lightman & Eardley 1976) when it was assumed that locally  $Q^+ \sim Q^-$  and thus  $f \rightarrow 0$ . While the model was successful in explaining observed hard X-rays from Cyg X-1, it turned out to be thermally unstable. Rees et al. (1982) proposed a hot ion torus model avoiding  $f$  to unity. In the similar spirit Narayan & Yi (1995) proposed the hot two temperature solution in the assumption of  $f \rightarrow 1$  including the strong advection into the flow. Abramowicz et al. (1995), based on the single temperature model, showed that the optically thin disc flow of accretion rate more than one Eddington does not have an equilibrium solution. However, they did not attempt to solve the complete set of differential equations. Based on some simplistic assumptions they showed the importance of advective cooling. Moreover, a single temperature description does not allow them to include all the underlying physics necessary to describe the cooling processes. In the due course, Mandal & Chakrabarti (2005) proposed a two temperature disc solution where the ion temperature could be as high as  $\sim 10^{12}$ K. However, they particularly emphasized on how does the shock in the disc flow enable cooling through the synchrotron mechanism, without carrying out a complete analysis of the dynamics. The present paper describes, to our knowledge, the first comprehensive work to model the two temperature accretion flow self-consistently by solving the complete set of underlying equations without any pre-assumptive choice of the flow variables to start with.

The generality lies not only in its construction but also its ability to explain the under-luminous to ultra-luminous sources, stellar mass to supermassive black holes. Table 3 lists the luminosities for a wide range of parameter sets, obtained by our model. It reveals that for a very low mass accretion rate  $\dot{M} = 0.0001$  around a supermassive black hole, the luminosity comes out to be  $L \sim 10^{34}$  erg/sec, which indeed is similar to the observed luminosity from a under-luminous source Sgr A\*. In other extreme, for  $\dot{M} = 100$  around a similar black hole,  $L \sim 10^{47}$  erg/sec, similar to what observed from the highly luminous AGNs like PKS 0743-67. On the other hand, when the black hole is considered to be of stellar mass, then at a high  $\dot{M} = 100$ , the model reveals  $L \sim 10^{40}$  erg/sec which is similar to the observed luminosity from ULX sources (e.g. SS433).

Table 3: Luminosity in erg/sec

$\dot{M}$	$M$	$\gamma$	$L$
0.0001	$10^7$	1.6	$10^{34}$
0.01	$10^7$	1.5	$10^{38}$
1	$10^7$	1.35	$5 \times 10^{42}$
100	$10^7$	1.34	$10^{47}$
0.01	10	1.5	$10^{33}$
1	10	1.35	$7 \times 10^{36}$
100	10	1.34	$10^{40}$

In general, an increase of accretion rate increases density of the flow which may lead to a high rate of cooling and thus decrease of the cooling factor  $f$ . Hence,  $f$  is higher, close to unity reassembling radiatively inefficient flows, for sub-Eddington accretors, and is lower, sometimes close to zero, for super-Eddington flows. Actual value of  $f$  in a flow also depends on the behaviour of hydrodynamic variables which determine the rate of cooling processes. Naturally, as the flow advances from the transition region to the event horizon,  $f$  varies between 0 and 1. However, if the black hole is considered to be rotating, the flow angular momentum decreases and thus the radial velocity increases. This in turn reduces the residence time of the sub-Keplerian flow hindering cooling processes to complete. This flow is then expected to be hotter and hence  $f$  to be higher compared to that around a static black hole. Therefore, the system may tend to be radiatively inefficient, even if its counter part around a static black hole appears to be an GAAF. However, this also depends on the value of  $\alpha$ , as shown in Fig. 18. A low value of  $\alpha$  increases the residence time of matter in the disc which helps in cooling processes to complete, rendering a radiatively inefficient flow to switch over to GAAF. This feature may help in understanding the transient X-ray sources.

In all the cases, the ion and electron temperatures merge or tend to merge at around transition radius. This is because, the electrons are in thermal equilibrium with the ions and thus virial around the transition radius, particularly when  $\dot{M} \geq 1$ . As the sub-Keplerian flow advances, the ions become hotter and the corresponding temperature increases, rendering the ion-electron Coulomb collisions weaker. The electrons, on the other hand, cool down via processes like bremsstrahlung, synchrotron emissions etc. keeping the electron temperature roughly constant upto very inner disc. This reveals the two temperature flow strictly.

Important point to note is that we have assumed throughout the coupling between the ions and electrons is due to the Coulomb scattering. However, the inclusion of possible nonthermal processes of transferring energy from the ions and electrons (Phinney 1981, Begelman & Chiueh 1988) might modify the results. However, as argued by Narayan & Yi (1995), the collective mechanism discussed by Begelman & Chiueh (1988) may dominate over the Coulomb coupling at either a very low  $\alpha$  or a very low  $\dot{M}$ . Instead, the viscous heating rate of ions is much larger than the collective rate of nonthermal heating of electrons, unless  $\alpha$  is too small what we have not considered in the present cases. Therefore, the assumption to neglect nonthermal heating of electrons is justified.

Now the future jobs should be to understand the radiation emitted by the flows discussed here and to model the corresponding spectra. This will be the ultimate test of the model in order to explain observed data.

## APPENDIX A: DISCUSSION OF BOUNDARY VALUES

We have four coupled nonlinear differential equations (6), (10), (12), (17) to be solved for  $\vartheta$ ,  $c_s$ ,  $\lambda$ ,  $T_e$ ; equations also involve  $\rho$  and  $P$ . To eliminate  $\rho$  and  $P$ , we use mass transfer equation (1) and equation of state (9). Therefore, in total we have five differential equations supplemented by an equation of state. Hence, we need five boundary conditions to start integration. Equation (1) can be integrated to obtain  $\dot{M}$  already given in Eqn. (2), which is supplied as an input parameter. Similarly, integrating Eqn. (10) we can obtain angular momentum flux

$$\dot{M}(\lambda - \lambda_{\text{in}}) = -4\pi x^2 |W_{x\phi}|, \quad (\text{A1})$$

where  $\lambda_{\text{in}}$  is the specific angular momentum at the inner edge of the disc, to be fixed by no torque inner boundary condition. Note that  $\lambda_{\text{in}} \leq \lambda_c$  (see, e.g., Chakrabarti 1996).

We therefore need the initial values of  $\vartheta$ ,  $c_s$ ,  $\lambda$  and  $T_e$  to solve the set of equations. When we impose the condition that the flow must pass through a critical radius  $x_c$  (around a sonic radius) where  $D = 0$ ,  $\vartheta$  and  $c_s$  at  $x_c$  are related by a quadratic equation of Mach number given by Eqn. (24).

For the continuity of  $d\vartheta/dx$ ,  $N = 0$  at  $x_c$ . Therefore, from  $N = 0$  which an algebraic nonlinear equation,  $c_s$  at  $x_c$  can be computed iteratively (using bisection method), which in turn fixes  $\vartheta$  at  $x_c$  as well, provided  $\lambda$  is known at that radius.

Now we need to set appropriate values of  $x_c$  and corresponding specific angular momentum  $\lambda_c$ . This is fixed iteratively by invoking the condition that the critical point to be saddle-type. This can be seen as follows. First we impose that  $\lambda_{\text{in}} = \lambda_c$ . Then by fixing the value of  $\lambda_c$  we find that if  $x_c$  is greater than a certain critical value  $x_{cc}$ , then the type of  $x_c$  changes from saddle-type to  $O$ -type which matter never can pass through. Figure A1a shows how the type of critical point and then solution topology change with a slight increase of  $x_c$ . On the other hand, as  $x_c$  decreases from  $x_{cc}$  which corresponds to the energy at  $x_c$  ( $E_c$ ) increases, the sub-Keplerian disc decreases in size. This advances the Keplerian disc. The reason is that increasing  $E_c$  corresponds to decreasing  $x_c$  and then increasing centrifugal energy ( $\lambda^2/2x_c$ ) which keeps



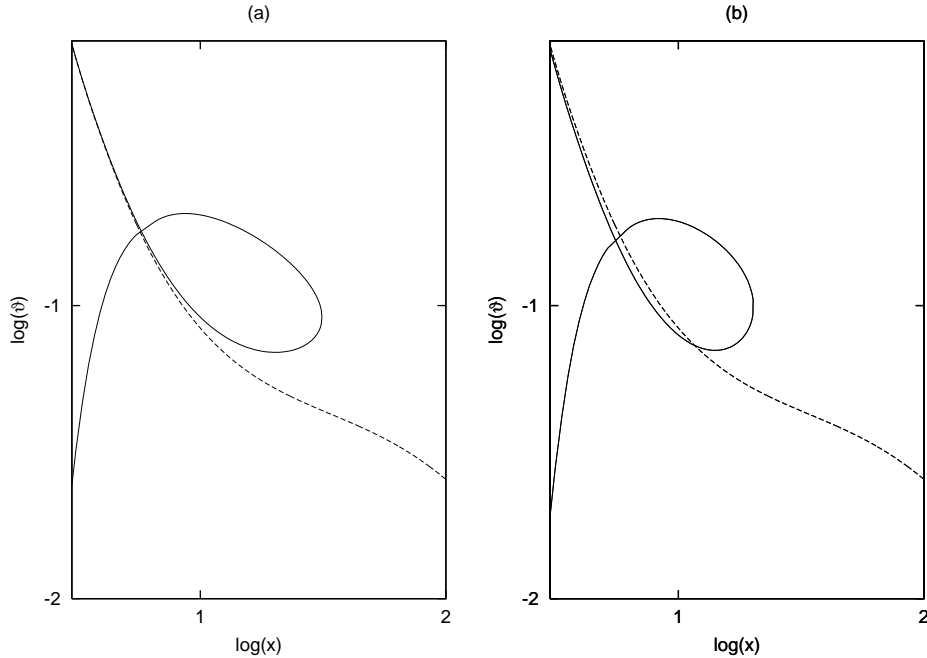


**Figure A1.** Comparison of the variation of radial velocity as a function of radial coordinate (a) between solutions with  $x_c = 5.5$  (dotted curve) and  $x_c = 5.7$  (solid curve), when  $\lambda_c = 3.2$ , (b) between solutions with  $\lambda_c = 3.2$  (dotted curve),  $x_c = 3.3$  (solid curve), when  $x_c = 5.5$ . Other parameters are same as that in Fig. 2 for  $M = 0.01$ .

the flow Keplerian until inner region. However, in principle the solution of the model equations is possible to obtain for any value of  $x_c$  from  $x_{cc}$  to the marginally bound orbit  $x_b$ .

Once  $x_c$  is fixed at  $x_{cc}$ , we have to obtain the best value of  $\lambda_c$ . By increasing the value of  $\lambda_c$  beyond a certain critical value  $\lambda_{cc}$  at a particular  $x_c$ , we again find a transition from saddle-type to  $O$ -type critical point. Figure A1b shows how the type of critical point and then solution topology change with a slight increase of  $\lambda_c$ . On the other hand, decreasing  $\lambda_c$  from  $\lambda_{cc}$  will tend the disc to more Bondi-type. Now for  $\lambda_{cc}$  we again have to obtain a new value of  $x_{cc}$  following the procedure outlined above and thereafter corresponding  $\lambda_{cc}$ . This needs to be continued iteratively until a specific combination of critical radius  $x_{cc}$  and corresponding specific angular momentum  $\lambda_{cc}$ , lying in a narrow range, is obtained which leads to a physically interesting large sub-Keplerian accretion disc, when matter infalling from a largest possible transition radius to a black hole event horizon through a saddle-type critical point. However, in principle the solution of the model equations is possible to obtain for a range of  $\lambda_c$  such that  $\lambda_{cc} \geq \lambda_c > 0$ .

There is, however, another initial value namely  $T_e$  at  $x_c$  ( $T_{ec}$ ) to be assigned. Choice of  $T_{ec}$  depends on the observed nonthermal radiation which restricts the value of  $T_e$  in general. But this restriction can only provide an order of magnitude of  $T_e$ . An exact value of  $T_{ec}$  should be obtained iteratively from a plausible range of  $T_e$  at  $x_c$  so that the values of  $x_{cc}$  and  $\lambda_{cc}$  obtained following the above mentioned procedure converge.

## APPENDIX B: COMPUTATION OF DERIVATIVE OF VELOCITY AT THE CRITICAL RADIUS

We first recall the derivative of velocity from Eqn. (20)

$$\frac{d\vartheta}{dx} = \frac{N(x, \vartheta, c_s, \lambda, T_e)}{D(\vartheta, c_s)}. \quad (\text{B1})$$

At the critical radius

$$\frac{d\vartheta}{dx} = \frac{0}{0}. \quad (\text{B2})$$

Therefore, we apply l'Hospital's rule and obtain

$$\begin{aligned} \frac{d\vartheta}{dx} &= \frac{\frac{D}{Dx} [N(x, \vartheta, c_s, \lambda, T_e)]}{\frac{D}{Dx} [D(\vartheta, c_s)]} \\ &= \frac{\frac{dN}{dx} + \frac{dN}{d\vartheta} \frac{d\vartheta}{dx} + \frac{dN}{dc_s} \frac{dc_s}{dx} + \frac{dN}{d\lambda} \frac{d\lambda}{dx} + \frac{dN}{dT_e} \frac{dT_e}{dx}}{\frac{dD}{d\vartheta} \frac{d\vartheta}{dx} + \frac{dD}{dc_s} \frac{dc_s}{dx}}. \end{aligned} \quad (\text{B3})$$

Now combining with Eqns. (26), (27), (28) we obtain

$$\frac{d\vartheta}{dx} = \frac{N_1 + N_2 \frac{d\vartheta}{dx}}{D_1 + D_2 \frac{d\vartheta}{dx}}, \quad (\text{B4})$$

where

$$N_1 = \frac{dN}{dx} + \frac{dN}{dc_s} \frac{J}{c_s} + \frac{dN}{d\lambda} \left( \frac{c_s^2 - 2\alpha J}{c_s} + \vartheta \right) + \frac{dN}{dT_e} \frac{(\Gamma_3 - 1)4\pi c_s x^{3/2}}{\dot{M} F^{1/2}} (Q^{ie} - Q^-) (1 - \Gamma_1) T_e \left( \frac{J}{c_s^2} + G \right), \quad (\text{B5})$$

$$N_2 = \frac{dN}{d\vartheta} + \frac{dN}{dc_s} \left( \frac{c_s}{\vartheta} - \frac{\vartheta}{c_s} \right) + \frac{dN}{d\lambda} \left( \frac{2\alpha x}{\vartheta c_s} \frac{I_{n+1}}{I_n} \left( \frac{c_s^3}{\vartheta} - \vartheta c_s \right) + \alpha x \right) + \frac{dN}{dT_e} (1 - \Gamma_1) T_e \frac{\vartheta}{c_s^2}, \quad (\text{B6})$$

$$D_1 = \frac{dD}{dc_s} \frac{J}{c_s} \quad (\text{B7})$$

$$D_2 = \frac{dD}{d\vartheta} + \frac{dD}{dc_s} \left( \frac{c_s}{\vartheta} - \frac{\vartheta}{c_s} \right). \quad (\text{B8})$$

Finally cross-multiplying in Eqn. (B4) we obtain a quadratic equation

$$D_2 \left( \frac{d\vartheta}{dx} \right)^2 + (D_1 - N_2) \left( \frac{d\vartheta}{dx} \right) - N_1 = 0 \quad (\text{B9})$$

such that

$$\left. \frac{d\vartheta}{dx} \right|_c = \frac{N_2 - D_1 \pm \sqrt{(D_1 - N_2)^2 + 4D_2 N_1}}{2D_2}, \quad (\text{B10})$$

where upper and lower signs correspond to wind and accretion respectively.

## ACKNOWLEDGMENTS

This work is partly supported by a project, Grant No. SR/S2HEP12/2007, funded by DST, India. One of the authors (SRR) thanks the Council for Scientific and Industrial Research (CSIR; Government of India) for providing a research fellowship. The authors also thank the referees for careful reading the manuscript and providing detailed reports which have helped to improve the paper.

## REFERENCES

- Abramowicz, M. A., Chen, X., Kato, S., Lasota, J.-P., Regev, O. 1995, ApJ, 438, L37.  
 Abramowicz, M. A., Czerny, B., Lasota, J. P., & Szuszkiewicz, E. 1988, ApJ, 332, 646.  
 Begelman, M. C. 1978, MNRAS, 184, 53.  
 Begelman, M. C., King, A. R., & Pringle, J. E. 2006, MNRAS, 370, 399.  
 Bisnovatyi-Kogan, G. S., & Lovelace, R. V. E. 2000, ApJ, 529, 978.  
 Chakrabarti, S. K. 1989, ApJ, 347, 365.  
 Chakrabarti, S. K. 1996, ApJ, 464, 664.  
 Chakrabarti, S. K., & Titarchuk, L. G. 1995, ApJ, 455, 623.  
 Chen, X., & Taam, R. E. 1993, ApJ, 412, 254.  
 Coppi, P. S. 1999, ASP Conference Series, 161, 375.  
 Eardley, D. M., & Lightman, A. P. 1975, ApJ, 200, 187.  
 Eggum, G. E., Coroniti, F. V., & Katz, J. I. 1985, ApJ, 298, 41.  
 Eggum, G. E., Coroniti, F. V., & Katz, J. I. 1988, ApJ, 330, 142.  
 Fabbiano, G. 2004, RMxAC, 20, 46.  
 Fabrika, S. 2004, ASPRv, 12, 1.  
 Ghosh, S., & Mukhopadhyay, B. 2009, RAA, 9, 157.  
 Gierliński, M., Zdziarski, A. A., Poutanen, J., Coppi, P. S., Ebisawa, K., & Johnson, W. N. 1999, MNRAS, 309, 496.  
 Gilfanov, M., Churazov, E., & Sunyaev, R. 1997, LNP, 487, 45.  
 Genzel, R., et al. 1998, ApJ, 498, 579.  
 Liang, E. P. T., & Thompson, K. A. 1980, 240, 271.  
 Lightman, A. P., & Shapiro, S. L. 1975, ApJ, 198, 73.  
 Lovelace, R. V. E., Romanova, M. M., & Newman, W. I. 1994, ApJ, 437, 136.  
 Mandal, S., & Chakrabarti, S. K. 2005, A&A, 434, 839.  
 Manmoto, T., Mineshige, S., & Kusunose, M. 1997, ApJ, 489, 791.  
 Matsumoto, R., Kato, S., Fukue, J., & Okazaki, A. T. 1984, PASJ, 36, 71.  
 Medvedev, M. V., & Narayan, R. 2001, ApJ, 554, 1255.

- Melia, F., & Misra, R. 1993, *ApJ*, 411, 797.
- Mineshige, S., Kawaguchi, T., Takeuchi, M., & Hayashida, K. 2000, *PASJ*, 52, 499.
- Muchotrzeb, B., & Paczynski, B. 1982, *AcA*, 32, 1.
- Mukhopadhyay, B. 2002, *ApJ*, 581, 427.
- Mukhopadhyay, B. 2003, *ApJ*, 586, 1268.
- Mukhopadhyay, B., & Ghosh, S. 2003, *MNRAS*, 342, 274; MG03.
- Nakamura, K. E., Kusunose, M., Matsumoto, R., & Kato, S. 1997, *PASJ*, 49, 503.
- Narayan, R., Kato, S., & Honma, F. 1997, *ApJ*, 476, 49.
- Narayan, R., Igumenshchev, I. V., & Abramowicz, M. A. 2000, *ApJ*, 539, 798.
- Narayan, R., & Popham, R. 1993, *Nature*, 362, 820.
- Narayan, R., & Yi, I. 1994, *ApJ*, 428, 13.
- Narayan, R., & Yi, I. 1995, *ApJ*, 452, 710.
- Novikov, I. D., & Thorne, K. S. 1973, in *Black Holes, Les Houches 1972 (France)*, ed. B. & C. DeWitt (New York: Gordon & Breach), 343.
- Paczynsky, B., & Wiita, P. J. 1980, *A&A*, 88, 23.
- Pringle, J. E., & Rees, M. J. 1972, *A&A*, 21, 1.
- Punsly, B., & Tingay, S. J. 2005, *ApJ*, 633, 89.
- Quataert, E., & Gruzinov, A. 2000, *ApJ*, 539, 809.
- Rajesh, S. R., & Mukhopadhyay, B. 2009, *New Astronomy* (to appear); arXiv:0908.3956.
- Rees, M. J., Begelman, M. C., Blandford, R. D., & Phinney, E. S. 1982, *Nature*, 295, 17.
- Shakura, N., & Sunyaev, R. 1973, *A&A*, 24, 337.
- Shapiro, S. L., Lightman, A. P., & Eardley, D. M. 1976, *ApJ*, 204, 187.
- Sinha, M., Rajesh, S. R., & Mukhopadhyay, B. 2009, *RAA* (to appear).
- Thorne, K. S., & Price, R. H. 1975, *ApJ*, 195, 101.
- Wallinder, F. H. 1991, *A&A*, 249, 107.
- Yuan, F. 1999, *ApJ*, 521, L55.
- Zdziarski, A. A., Grove, J. E., Poutanen, J., Rao, A. R., & Vadawale, S. V. 2001, *ApJ*, 554, 45.